Article

Active Collapse in the Central Betic Cordillera: Development of the Extensional System of the Granada Basin

Asier Madarieta-Txurruka [1], José A. Peláez [2,*], Lourdes González-Castillo [1], Antonio J. Gil [3,4] and Jesús Galindo-Zaldívar [1,5]

[1] Department of Geodynamics, University of Granada, 18071 Granada, Spain; amadatxu@ugr.es (A.M.-T.); lgcastillo@ugr.es (L.G.-C.); jgalindo@ugr.es (J.G.-Z.)
[2] Department of Physics, University of Jaén, 23071 Jaén, Spain
[3] Department of Cartographic, Geodetic and Photogrammetry Engineering, University of Jaén, 23071 Jaén, Spain; ajgil@ujaen.es
[4] Center for Advanced Studies in Earth Sciences, Energy and Environment (CEACTEMA), University of Jaén, 23071 Jaén, Spain
[5] Andalusian Earth Sciences Institute, Spanish National Research Council (CSIC), University of Granada, 18100 Armilla, Spain
[*] Correspondence: japelaez@ujaen.es

Abstract: The Betic Cordillera was formed by the collision between the Alboran Domain and the South Iberian paleomargin in the frame of the NW–SE convergent Eurasia–Nubia plate boundary. The central region is undergoing a heterogeneous extension that has not been adequately analysed. This comprehensive study addressed it by collecting structural geologic, seismologic, and geodetic data. The region west of the Sierra Nevada is deformed by the extensional system of the Granada Basin, which facilitates E–W to NE–SW extension. Moreover, the southern boundary of Sierra Nevada is affected by a remarkable N–S extension related to E–W normal to normal–dextral faults affecting the shallow crust. However, geologic and geodetic data suggest that the western and southwestern Granada Basin boundary constitutes a compressional front. These data lead to the proposal of an active extensional collapse from the uplifted Sierra Nevada region to the W–SW–S, over an extensional detachment. The collapse is determined by the uplift of the central Betics and the subsidence in the Alboran Basin due to an active subduction with rollback. Our results indicate that the central Betic Cordillera is a good example of ongoing extensional collapse in the general context of plate convergence, where crustal thickening and thinning simultaneously occur.

Keywords: active tectonics; extensional collapse; stress tensors; GNSS; central Betic Cordillera; Granada Basin

1. Introduction

Mountain ranges, such as the Betic Cordillera in the westernmost Mediterranean, are characterized by lateral variations in crustal and lithospheric thickness due to convergence and related mountain-building processes. Consequently, much of the extensional tectonics occurring in regions with thickened crust aim to balance the excess or deficiency of gravitational potential energy [1] and are commonly referred to as gravitational collapses [2] or extensional collapses [3]. Such collapses can be synorogenic or postorogenic, depending on whether extension occurs concurrently with ongoing thickening or after mountain building, respectively [4]. Two distinct modes of flow are observed during extensional collapse: "fixed-boundary collapse" and "free-boundary collapse" [1]. In the former, extensional deformation affects the thickened regions simultaneously with the deformation of the surrounding thinner regions. The Tibetan Plateau serves as a prominent example of fixed-boundary collapse, where extensional detachment and ductile thinning of the lower crust occur alongside thrusting at the thinner boundaries [5–9]. On the other hand, free-boundary collapse is primarily associated with a change in plate motion, transitioning from

a convergent plate boundary to a divergent plate one, as occurred in the Basin and Range Province tectonics setting (western United States and northwestern Mexico) [3,10,11].

The alpine Betic Cordillera constitutes the northern branch of the Gibraltar Arc, which formed in the frame of the N–S to NW–SE convergence along the E–W Eurasia–Nubia plate boundary in the westernmost Mediterranean Sea. The development of the arc since the Miocene is the result of the westward migration of the Alboran Domain driven by subduction with rollback [12,13]. This phenomenon produced an E–W extension of the Alboran Domain in the Betic Cordillera while the collision with the South Iberian Domain was taking place [14–18]. Extension facilitated the exhumation of the Nevado-Filábride complex [19] below the Mecina extensional detachment with top-to-W displacement [20–22]. From the Tortonian onwards, the NNW–SSE convergence generated large E–W folds accentuating the domal structures and individualising the intramontane basins in the synclines and in the grabens [23–27], including the Granada Basin.

Nowadays, the south–central region of the Betic Cordillera (Figure 1) is one of the most seismically active regions in the entire Iberian Peninsula [12]. Despite the NNW–SSE convergence [28,29] both seismicity and GNSS data indicate a heterogeneous E–W to NE–SW extension affecting the shallow crust [16] west of the Sierra Nevada Dome [29–32]. To the west of the Sierra Nevada, the Granada Basin extensional system (Figures 1 and 2) accommodated the E–W to NE–SW extension by high-angle normal faults over active extensional detachments [17,18]. However, the propagation of active deformation towards the southwest and south of the Granada Basin and Sierra Nevada areas has not been adequately analysed in detail.
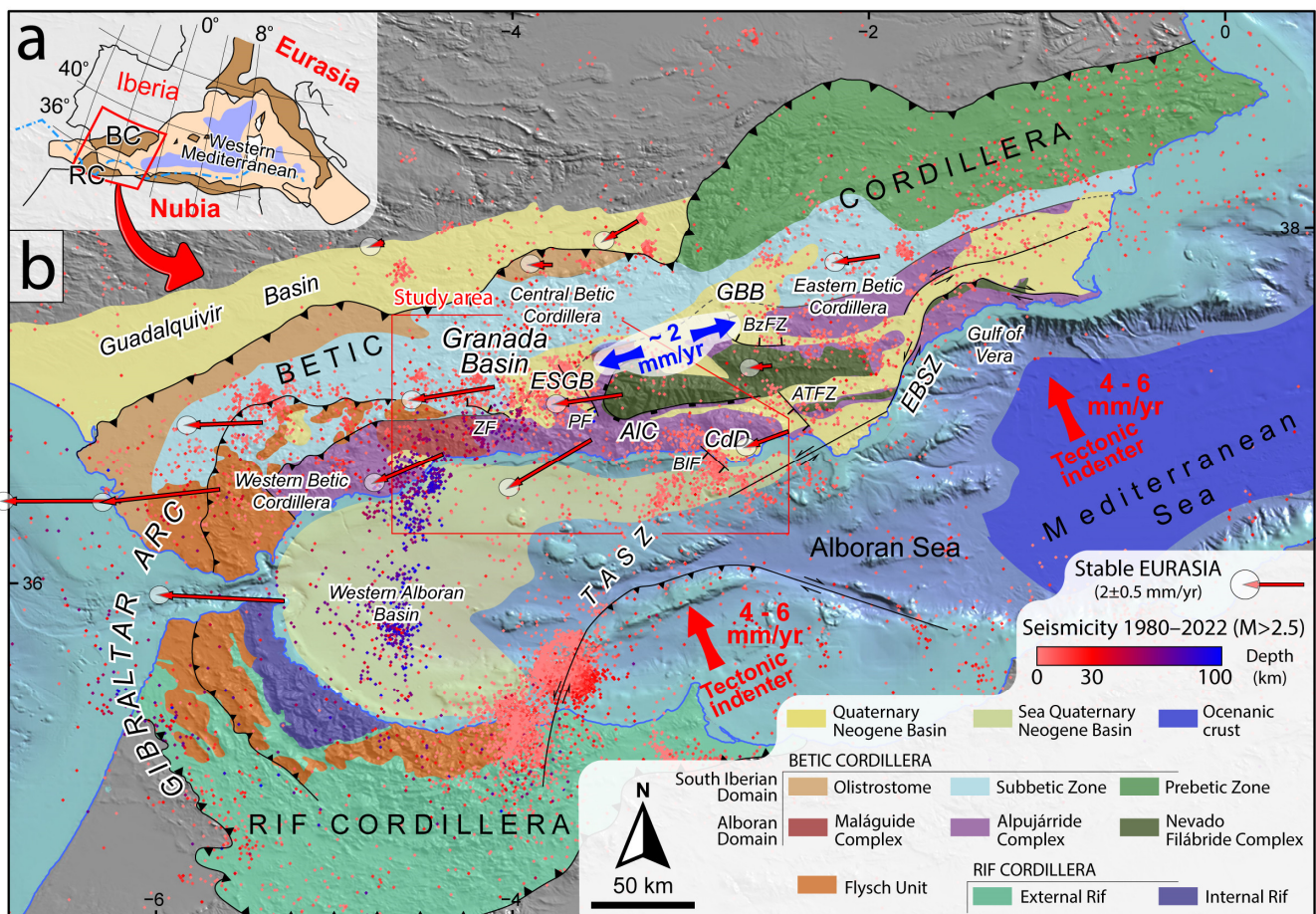

Figure 1. Geological and tectonic setting of the Betic and Rif Cordillera forming the Gibraltar Arc. (**a**) Sketch of the western Mediterranean Alpine Mountain belts. Dark brown: onshore Alpine Belt.

Light brown: offshore Alpine Belt. Blue: Cenozoic oceanic crust. BC: Betic Cordillera. RC: Rif Cordillera. (**b**) Simplified geologic map of the Gibraltar Arc. Seismicity since 1980 and M > 2.5 taken from IGN [33] and GNSS data [31,34] are shown. Red arrows show the Eurasia–Nubia convergence [28], and blue arrows represent the extension of the central Betic Cordillera [29]. GBB: Guadix–Baza Basin. AlC: Alpujarras Corridor. CdD: Campo de Dalías. TASZ: Trans-Alboran Shear Zone. EBSZ: Eastern Betic Shear Zone. ESGB: Extensional system of the Granada Basin. ZF: Zafarraya Fault. PF: Padul Fault. BlF: Balanegra Fault. BzFZ: Baza Fault Zone. ATFZ: Almería Tabernas Fault Zone.
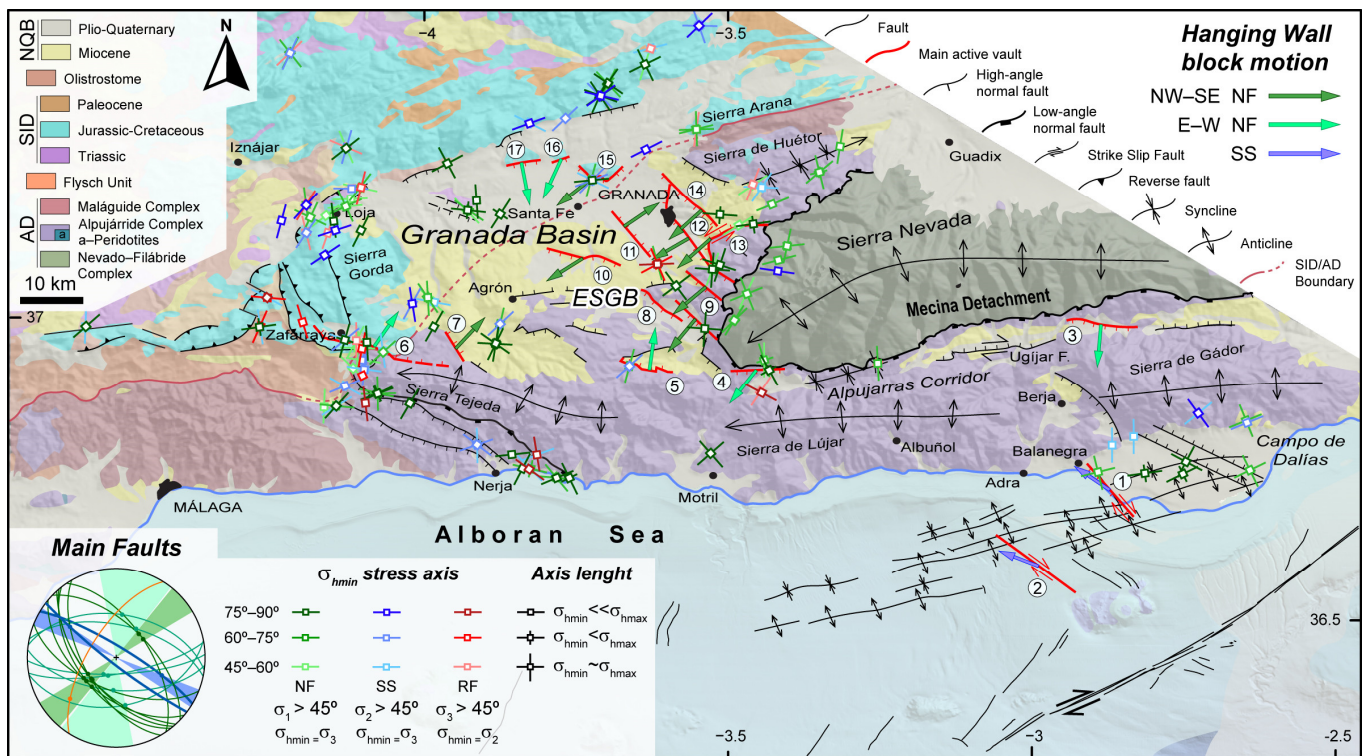

Figure 2. Geological map of the central Betic Cordillera including the Granada Basin, modified from [17,35–39]. ESGB: Extensional system of the Granada Basin; AD: Alboran Domain; SID: South Iberian Domain; NQB: Neogene–Quaternary Basin. The main active faults and their hanging wall block motion (top-right legend) are taken from the Quaternary Active Fault Database of Iberia (QAFI) [40] and are indicated by circled numbers corresponding to Table 1. NF: Normal fault. SS: Strike-slip fault. The minimum horizontal stress axes of the latest paleostresses obtained from striated microfaults are shown (bottom left legend) [41–46]. Green axes indicate normal faulting (NF), which is defined by a σ_1 dipping more than 45°. Blue axes indicate strike-slip faulting (SS), which is defined by a σ_2 dipping more than 45°. Red axes indicate reverse faulting (RF), which is defined by a σ_3 dipping more than 45°. The greater the intensity of the colour of the axis, the closer to 90° of σ_1 in NF, σ_2 in SS, and σ_3 in RF. The minimum horizontal stress axes correspond to a σ_3 in normal (NF) and strike-slip faulting (SS) and to a σ_2 in reverse faulting (RF). In the case of normal faulting and prolate stress ellipsoid, both σ_2 and σ_3 are considered as σ_{hmin}. In the cases of reverse faulting and oblate ellipsoid, no axis is considered as σ_{hmin}.

Table 1. Orientation and kinematics of the main active faults.

N	Fault Name	Strike (N°E)	Dip (°)	Dip Direction	Rake (°)	Quaternary Activity Evidence
1	Balanegra	150	60	SW	−135	(1) Rectilinear scarps with staircase morphology that influence the drainage network and control the coastline of Campo de Dalías. (2) Holocene asymmetric clastic wedges and cut sediments. (3) Seismites in Quaternary sediments.
2	Adra	121	80	SW	−135	Surface expression, offset Quaternary horizons, seismicity (1910 Adra earthquake).
3	Laujar de Andarax	95	60	S	−90	The fault produces a sharp mountain front and small topographic scarps that continue for hundreds of meters.
4	Lanjarón	88	75	S	−102	The general line of the fault with the scarp visible in some places.
5	Albuñuelas	278	50	N	−90	The line of the fault, and at some points, the surface of the scarp.
6	Zafarraya	282	60	N	−102	Straight mountain front, wind gap, conspicuous fault scarp, paleoearthquake features, association with 1884 Arenas del Rey event.
7	Játar	314	60	NE	−90	The general scarp.
8	Padul–Nigüelas	130	55	SW	−90	Very well-expressed triangular facets, fault scarps, and recent peat layers tilted towards the fault. Horizontal slip calculated by local GNSS network.
9	Dílar	140	60	SW	−90	Splendid scarp and other associated features.
10	Malahá	112	60	SW	−110	Linear break in the landscape with associated mountain front. Traceable fault surface. Related archaeological evidence.
11	Santa Fe	326	60	NE	−90	A linear change of relief
12	Granada	150	60	SW	−90	The scarp is only well-conserved at some points. Vertical slip calculated by high-precision levelling lines.
13	Huenes	212	65	NW	−35	The scarp with many indicators of sense of displacement
14	El Fargue	138	60	SW	−90	The scarp and the line of the fault.
15	Sierra Elvira	142	55	SW	−90	Well expressed scarp, minor structures related, geomorphic features.
16	Obeilar–Pinos Puente	80	75	S	−100	A general and linear change of relief.
17	Tocón–Obeilar	79	45	S	−90	It has scarce geomorphic evidence.

Data collected mainly from Quaternary Active Database of Iberia (QAFI) [40,47].

This contribution aimed to analyse in detail the heterogeneous extensional tectonics of the Granada Basin and its propagation towards the surrounding areas of the central Betic Cordillera. To this aim, a comprehensive compilation of existing and new geological, seismological, and geodetic data was conducted. A new tectonic model is proposed to enhance understanding of the ongoing tectonic evolution in this complex region of the western Mediterranean. This model can serve as a valuable reference for future investigations in similar tectonic settings worldwide.

2. Geological Setting

The Betic Cordillera (Figure 1) is one of the mountain ranges surrounding the westernmost Mediterranean (Figure 1a) and, together with the Rif Cordillera, forms the Gibraltar Arc (Figure 1b). It is divided into two main domains separated by the Flysch Unit (Figure 1) [48]. To the north, the South-Iberian Domain is formed by the External Thrust and Fold Belt affected by thin-skinned tectonics, being composed of sediments from the extended continental margin [49–51]. The Prebetic Zone, currently outcropping better in the east, corresponds to the continental platform [18], while the Subbetic Zone, now

outcropping better towards the west, was the hyperextended margin [49]. To the south and southeast, the Alboran Domain is mainly formed by three metamorphic complexes distinguished by their stratigraphy, metamorphism, and structural position [52]. From top to bottom, these complexes are the Maláguide Complex; the Alpujárride Complex, including the Ronda Peridotites [53]; and the Nevado–Filábride Complex [18]. The Neogene–Quaternary sediments are located above these domains (Figure 1b). The Western Alboran Basin [54] and the Guadalquivir Foreland Basin [55] are the main basins. Finally, some intramontane basins developed, such as the Granada and Guadix–Baza basins (Figure 1) [56].

Deformation in the Betic Cordillera began during the Paleocene–Eocene epoch [57], involving shortening and significant dextral displacement between the Alboran and South Iberian domains [23]. After that, during the early Miocene, the Betic Cordillera experienced the main shortening and back-arc extension [58,59]. The Alboran Domain was subjected to intense extension, leading to crustal thinning, the exhumation of metamorphic complexes, and the formation of low-angle normal faults. These low-angle faults separated the main metamorphic complexes: the Maláguide-Alpujárride brittle extensional contact during the Burdigalian–Langhian [60], and after that, westward-directed Mecina extensional detachment caused the exhumation of the metamorphic Nevado–Filábride Complex [22,25,26,61]. Following this event, stretching continued in an E–W to ENE–WSW direction with a top-to-west sense of shear, resulting in the formation of a-type dome metamorphic core complexes and leading to the initiation of intramontane basins [62,63]. Dextral strike-slip faults developed south of the Sierra Nevada dome, resulting in the Alpujarras Corridor [64], and to the north along the contact between the Alboran and South Iberian domains [65,66]. Meanwhile, thrusting affected the South Iberian domain [14], forming a fold-and-thrust belt due to the thrusting of the Alboran Domain over the Iberian margin [50,67]. In the central Betics, the main shortening happened between the Aquitanian and Burdigalian, evidenced by thin-skinned style deformation [68,69]. The Guadalquivir Basin started developing in the Langhian [70]. Later, the Betic Cordillera mountain front was affected by N–S extension [23] related to gravitational dismantling by WNW–ESE normal faults until the Serravallian [71]. Simultaneously, to the north of the Granada Basin, N–S normal faults accommodated arc-parallel extension [72] related to the westward displacement in the Alboran Domain [71,73]. To the west of the Granada Basin, westward-verging thrust activity connected with the Mecina detachment was reported [17].

The Eurasia–Nubia NW–SE convergence and orthogonal extension have affected the Betic Cordillera since the Tortonian. In the Alboran Domain, the development of NE–SW and E–W folds amplified the domal geometry of the Sierra Nevada [24,35]. Meanwhile, NE–SW orthogonal extension continued producing NW–SE normal faults, conjugated E–W oriented dextral and normal faults, and NE–SW sinistral to normal faults, individualizing the Neogene–Quaternary basins [23,35]. In the South Iberian Domain, the NW-directed shortening continued [73] with the progression of the deformation and north-westward migration of the Guadalquivir Basin [72]. Meanwhile, NW–SE to N–S faults accommodated the arc-parallel extension [74].

Many models have been proposed to understand the recent evolution of the Betic Cordillera. They can be summarized into two main groups. (i) Delamination models [14,15,75–77] suggest an orogenic root that becomes detached through lithospheric delamination [15,76] or mantle convection [14] during the Eurasia–Nubia convergence in Late Oligocene or Early Miocene. This lithospheric removal caused a radial crustal extension that ended in the Late Miocene due to the dominance of the Eurasia–Nubia convergence [75]. (ii) Subduction models of lithosphere below the Alboran Domain present many variations considering rollback and/or slab detachment [78–82]. The subduction begins due to a northward dipping slab attached to the African margin, which later was fragmented. The Alboran Domain moved westward associated with the rollback of one slab fragment [78,79,82,83]. The westward tearing detached the northward dipping slab from Africa, while in the Iberian margin, it is still partly attached. In the western Betic Cordillera,

the slab is dipping eastward to south-eastward [84–86], while in the central and eastern Betic Cordillera, it is detached due to slab tearing [81]. In this view, the Alboran Basin was formed due to the back-arc extension [87]. Some hypotheses suggest that subduction with rollback continues to be active today in the western Betic Cordillera [34,80,88,89]. In addition, Duggen et al. [90,91] proposed that the delamination of the continental Alboran lithosphere was driven by the subduction of the oceanic lithosphere. This model is consistent with a slab rollback of an east-dipping slab beneath the Alboran Sea [92], resulting in the delamination of the Alboran lithosphere during the Late Miocene and its replacement by an asthenospheric plume.

The current evolution of the Betic Cordillera is driven by a 3–5.6 mm/year westward migration [34,93] and clockwise rotation [30] of the northern branch of the Gibraltar Arc with respect to Eurasia and a simultaneous NW–SE convergence of 4–6 mm/year along the Eurasia–Nubia plate boundary, oblique to its E–W regional trend [28], affecting the region heterogeneously (Figure 1b). In the western Betic Cordillera, the westward migration of the arc is accommodated by active folding [94] and faulting [95], as observed in regional geodetic studies [30,34,93]. In the eastern Betic Cordillera, the convergence is transferred through the Trans-Alboran Shear Zone [96,97], a transpressive tectonic corridor that continues onshore as the Eastern Betic Shear Zone (Figure 1b) [98]. This is a consequence of the movement towards the NW of a tectonic indenter located in the Gulf of Vera (Figure 1) [99,100]. In the central Alboran Sea, the NW–SE compression is due to the north-westward movement of another tectonic indenter (Figure 1b) [36], generating strike-slip faulting and affecting the coastal areas to the south of Sierra Nevada [101]. On the contrary, the Alboran Domain in the central Betic Cordillera is affected by a NE–SW to ENE–WSW extension of nearly 2 mm/year (Figure 1b) [29]. Finally, the South Iberian Domain in the central Betics presents a 1 mm/year westward displacement with respect to the stable Iberia [31], but no extension has been registered [30].

The ENE–WSW extension in the central Betic Cordillera (Figures 1 and 2) is mainly accommodated by NW–SE extensional fault zones, primarily affecting the Alboran Domain [35]. The main ones include the Baza Fault zone in the northeast [102], the Almería–Tabernas Fault zone in the east [103], the Balanegra Fault in the south [101], and the extensional system of the Granada Basin in the west (Figure 1b) [104]. The extensional system of the Granada Basin (Figures 1 and 2) accommodates the extension of the central Betic Cordillera [30,105] and affects the upper crust of the Alboran Domain as well as the South Iberian Domain, rooting into a detachment zone at a depth of approximately 10–15 km [104]. The active detachment has been considered the western continuation in the depth of the Mecina detachment [20,106]. The western boundary of the Granada Basin is subject to both compressional and strike-slip faulting (Figure 2) [37,107–109]. The Campo de Dalías and the adjacent Alboran Sea are affected by NW–SE normal dextral faults, such as the Balanegra Fault, and ENE–WSW folds (Figure 2) [38,101,110–112]. The connection zone between the seismogenic areas of the Granada Basin and the Campo de Dalías is hardly affected by seismicity (Figure 1b). There, the synformal area called the Alpujarras Corridor has been interpreted as a dextral fault zone with related normal and reverse faulting (Figure 2) [31,64,113].

3. Methodology

This study compiled knowledge of the tectonic structures from the Granada Basin to the Campo the Dalías to frame this sector within the current evolution of the Betic Cordillera (Figure 2). The former was addressed through the integration of existing and new geological, seismological, and geodetical data.

The geological data included the geometry of structures, kinematic data, and paleostress determinations from the latest faults. The main active fault data were taken from the Quaternary Active Fault Database of Iberia (Figure 2 and Table 1) which considers the fault described as active in indexed publications [40,47]. To determine the latest paleostresses, we summarized all data on brittle structures with evidence of recent activity. Orientation data

from striated microfaults (Figures 2 and 3 and Tables 2 and S1) provided information about the stress ellipsoid that was active in the region [114]. These data were taken from López-Chicano [41], Galindo-Zaldívar et al. [42,43], Ruano [44,45], and Reicherter and Peters [46] and were calculated using the methods of Etchecopar et al. [115] and Galindo-Zaldívar and González-Lodeiro [116].
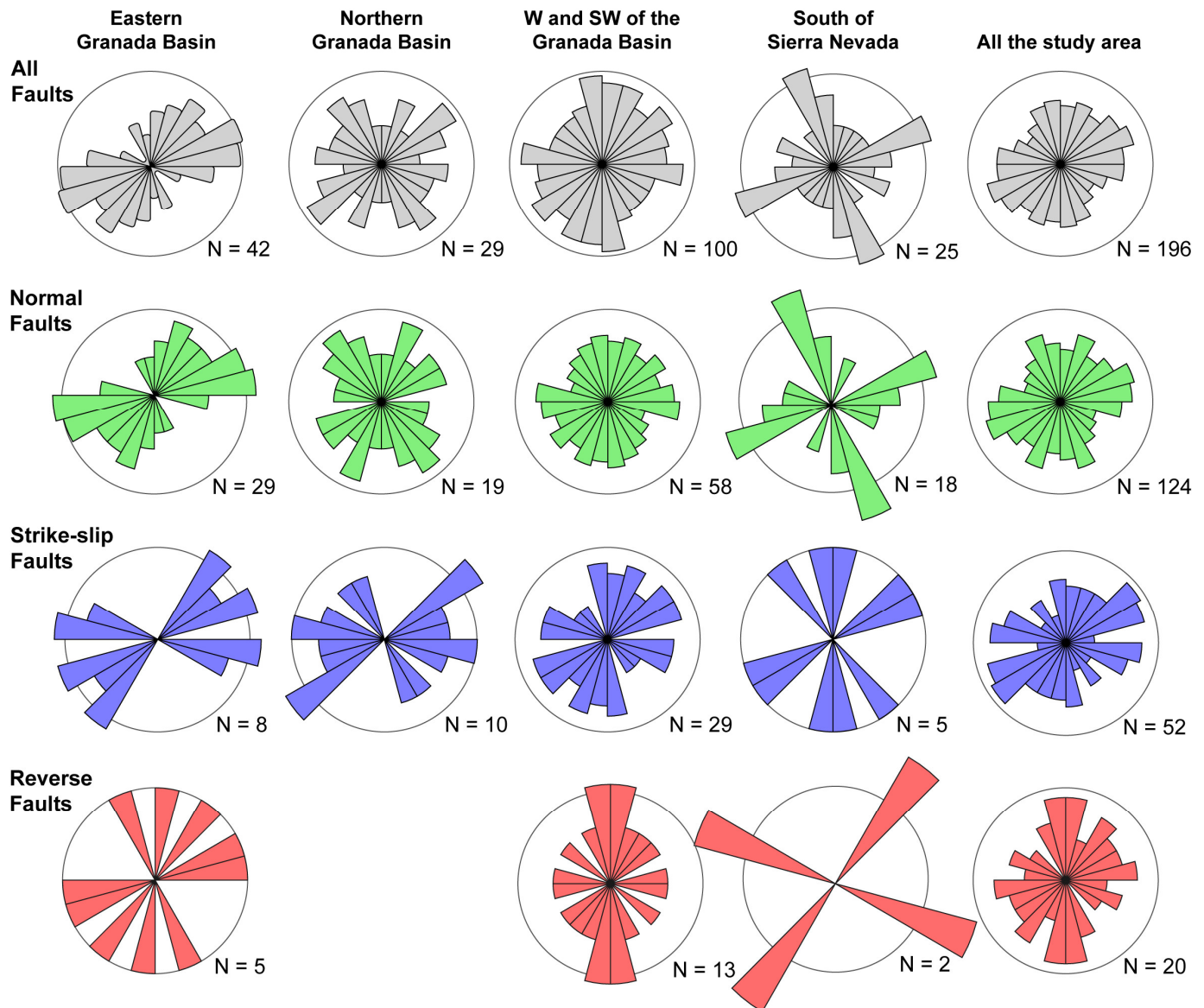

Figure 3. Rose diagrams of minimum horizontal stress axis (σ_{hmin}) in each sector and type of faulting [41–46]. Grey: all data together; green: normal faulting; blue: strike-slip faulting; red: reverse faulting. The minimum horizontal stress axes correspond to a σ_3 in normal and strike-slip faulting, and to a σ_2 in reverse faulting. In the case of σ_1 vertical and prolate stress ellipsoid, both σ_2 and σ_3 are considered as σ_{hmin}. In the case of σ_3 vertical and oblate ellipsoid, no axis is considered as σ_{hmin}.

Table 2. Type of faulting for each study sector.

	Normal Fault		Strike-Slip Fault		Reverse Fault		All
	N	%	N	%	N	%	N
All	97	55	52	30	26	15	175
Eastern Granada Basin	26	67	8	20	5	13	39
Northern Granada Basin	13	54	10	42	1	4	24
W and SW Granada Basin	48	51	29	31	17	18	94
South of Sierra Nevada	10	56	5	28	3	16	18

Data collected from [41–46].

The seismological data consisted of recent seismicity, earthquake focal mechanisms, and stress tensors obtained from earthquake focal mechanism solutions (Figure 4). Seismicity was obtained from the seismic catalogue of the Spanish Instituto Geográfico Nacional (IGN), which provides information about the zones with the most active brittle deformation [33]. Focal mechanisms report on active structures at depth and are used to determine present-day stresses [117,118]. The M > 4.5 earthquake focal mechanism solutions are depicted in Figure 4. The reduced stress tensors (Table 3) calculated for the eastern Granada Basin [104,119] using the Win-Tensor™ code developed by Delvaux and Sperner [120] and Delvaux and Barth [121] were also considered. Moreover, the reduced stress tensors of the intermediate seismicity [88] were calculated using FSA software [122,123]. We also considered the results of the right dihedra diagrams [117] from the 1988 Agrón series in the central Granada Basin [43], the westernmost Granada Basin [44], the Campo de Dalías–Northern Alboran Sea [38], and intermediate seismicity [88].
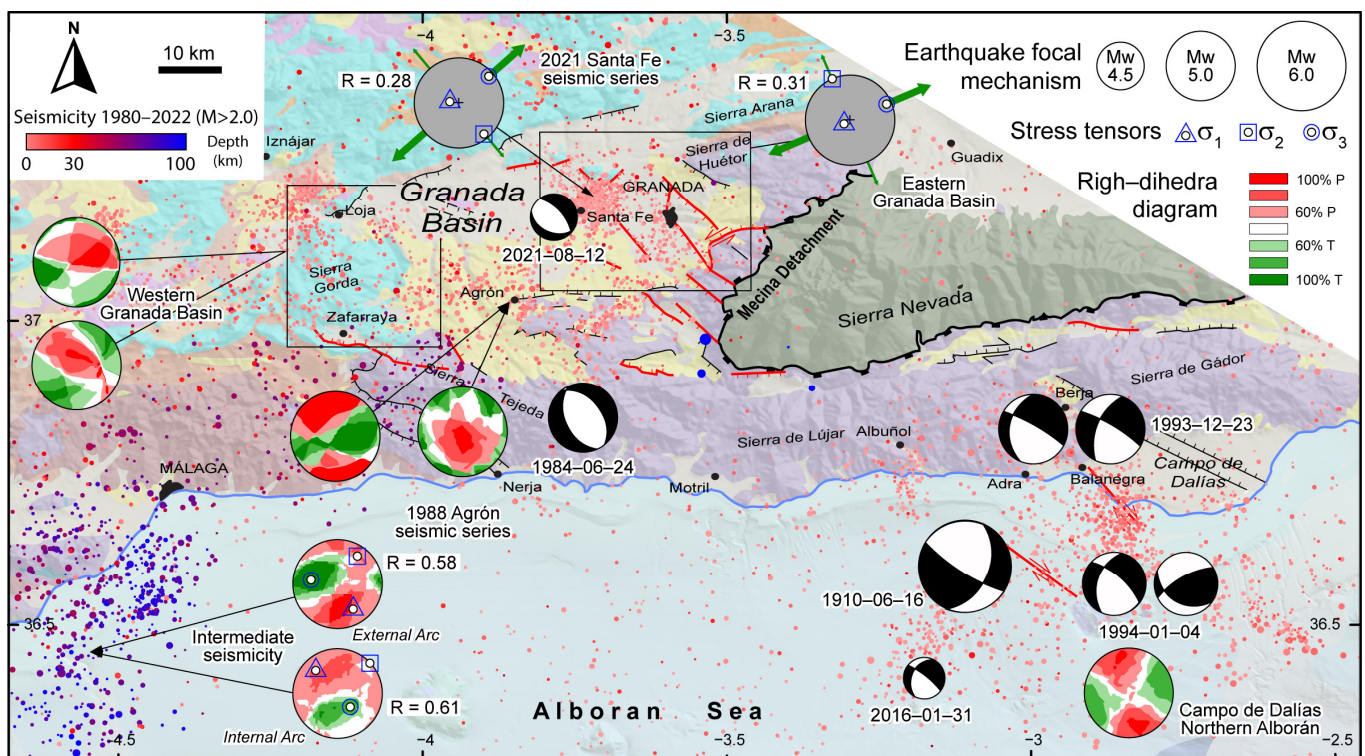

Figure 4. Seismological data of the central Betic Cordillera. The seismicity since 1980 was taken from Spanish IGN. Reduced stress tensors [88,104,119], right dihedra diagrams [38,43,44,88], and earthquake focal mechanism with M > 4.5 are shown [124–128]. R indicates the axial ratio defined by R = $(\sigma_2 - \sigma_3)/(\sigma_1 - \sigma_3)$.

Table 3. Reduced stress tensors of the central Betic Cordillera.

	S1	S2	S3	R	Reference
Eastern Granada Basin	78/240	01/336	12/067	0.31	[104]
2021 Santa Fe seismic series	74/277	12/141	11/049	0.28	[119]
External Arc	37/147	27/035	41/278	0.58	[88]
Internal arc	33/316	02/047	57/139	0.61	

R indicates the axial ratio.

GNSS networks are highlighted as the best geodetic technique [129] to study regional active surface deformations on a millimetre scale [130,131]. The geodetic data included GNSS data taken from both continuous and survey mode networks (Figure 5). The continuous sites of the central Betic Cordillera (NEVA, LOJA, PALM, and MALA) are part of the Iberian and North Morocco regional network deployed by the Topo Iberia project [31]. The survey-mode GNSS data are part of the Padul Fault network [132], Campo de Dalías network [101], and central Betic Cordillera Extensional network [133]. Since the Padul network is highly localized, the mean value for the sites located within the hanging wall block of the Padul Fault was considered [132]. In this study, the Sierra Nevada was considered a relatively stable block of the central Betic Cordillera due to its limited seismic activity and minimal affection by major faults. Consequently, to assess recent surface deformation above the Nevado–Filábride Complex, the velocity vectors with respect to the NEVA geodetic site were computed.
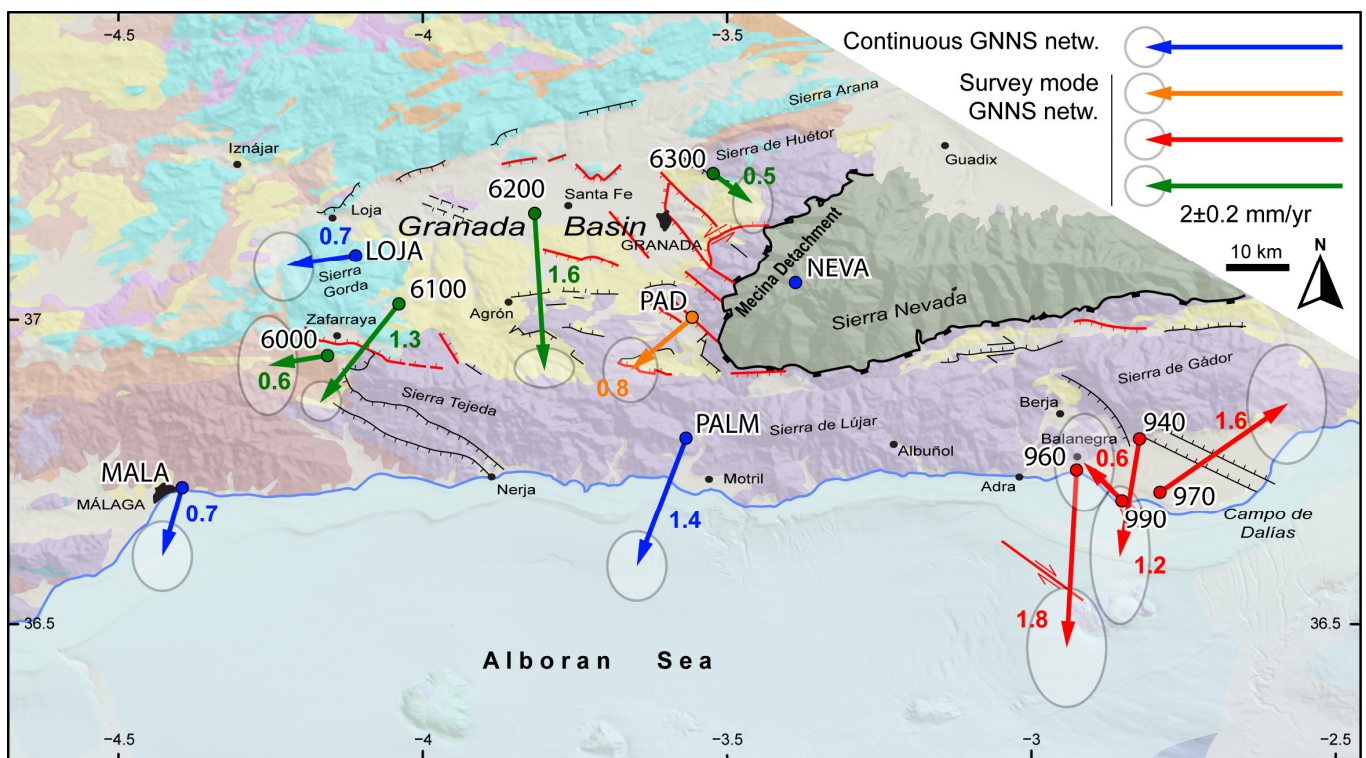

Figure 5. GNSS velocity field with respect to the fixed NEVA. The numbers show the velocity rate in mm/year. Blue arrows belong to the Iberia–North Morocco continuous GNSS network [31]. The orange arrow is the mean value of the sites located in the hanging wall block of the Padul Fault [132]. Red arrows belong to the Campo de Dalías survey-mode network [101]. Green arrows belong to the central Betic Cordillera extensional survey-mode network [133]. Each GNSS site maintains its original name as a reference.

4. The Recent and Active Deformation and Stresses of the Granada Basin and Surrounding Regions

4.1. Structural Data

4.1.1. Main Active Faults

The main active faults of the central Betic Cordillera (Figure 2 and Table 1) are situated in the eastern Granada Basin. They strike N130°–150° E and present normal kinematics, showing an N40°–60° E extension. Most of these faults dip to the southwest, but antithetic faults are also present. Notable faults are the Granada Fault, with vertical slips of up to 1 mm/year [104]; the Padul Fault, with a horizontal extension of 0.5 mm/year [132]; and the Sierra Elvira faults, which hosted the 2021 Granada seismic series [119]. In addition, there are ENE–WSW active faults located on the northern edge of the Granada Basin, such as the Tocón–Obeilar and the Obeilar–Pinos Puente Faults. Moreover, the Huenes Fault stands out in the southeastern edge with a NE–SW direction and a main sinistral component, compatible with the NE–SW to ENE–WSW extension. Moving westward, the Zafarraya Fault is the primary active fault located in the southwestern Granada Basin. It strikes E–W and dips to the north with normal to normal–dextral kinematics. It is considered to be the source of the 1884 Andalusian earthquake [134], as its activity is associated with an active folding [35,37]. To the south of the Sierra Nevada, the Lanjarón and Laujar de Andarax Faults are located in the Alpujarras Corridor, striking E–W and dipping to the south [135,136]. The N–S direction of extension is due to the activity of the ENE–WSW-striking Tocon–Obeilar Fault north of the Granada Basin and the E–W Laujar de Andarax Fault south of Sierra Nevada. The NNW–SSE direction of extension occurs in E–W faults with normal–dextral kinematics, such as the Zafarraya, Albuñuelas, and Lanjarón Faults. Finally, other active NW–SE trending faults are located to the west of Campo de Dalías, showing a NE–SW extension. Both the Balanegra and Adra Faults present a main dextral component in addition to a normal behaviour (Table 1).

4.1.2. Latest Paleostresses

The analysis of the latest paleostress field allows for an understanding of the stress state in a certain region and, therefore, the behaviour of recent deformations (Figures 2 and 3 and Tables 2 and S1). Most of the stress data in the central Betic Cordillera are dominated by a subvertical σ_1, leading to the most common normal faulting. We chose to represent the main trends of extension σ_{hmin} for each station (Figure 3).

Extension varies in the different sectors of the study area (Figure 3). The eastern Granada Basin is dominated by normal faulting, and all the types of striated microfaults indicate a NE–SW to ENE–WSW extension. The northern part of the basin is affected by normal faults inducing both NE–SW and NW–SE extension, while the strike-slip faults indicate a NE–SW extension. The W and SW of the Granada Basin is also dominated by normal faulting, although strike-slip and reverse faulting are also present. Both normal and strike-slip faulting indicate radial extension with a lack of NW–SE extension. The reverse faulting is concentrated around Zafarraya (Figure 2). It indicates a main E–W compression and perpendicular extension. Finally, the sector located between the Sierra Nevada and the coast is dominated by normal faulting and some strike-slip faulting occurring in Sierra de Gádor. The horizontal minimum stresses indicate a NNE–SSW and ENE–WSW extension.

4.2. Seismological Data

4.2.1. Seismicity

The Betic Cordillera (Figure 1) is a major seismic zone in the Iberian Peninsula. The central Betic Cordillera (Figure 4) experiences shallow seismicity primarily located in the Granada Basin and the Campo de Dalías areas. The Granada Basin is characterized by recurrent low and low-to-moderate seismicity, with the occurrence of seismic series such as the 1988 Agrón series and the 2021 Santa Fe series [43,119,124]. Seismic activity is mainly concentrated in the eastern and southern edges. To the west of the Granada Basin, northwest of the Sierra Gorda, shallow seismicity is also recurrent, and seismic series usually occur

here, such as the 1985 Loja series [137] and the 1998 Iznájar series [108]. In the southwestern Granada Basin, some moderate historical earthquakes have happened, notably the 1884 Andalusian earthquake [134,138]. The Campo de Dalías and the adjacent Alboran Sea is another sector where shallow low and low-to-moderate seismicity is recurrent. This area is also affected by seismic series, such as the 1993–1994 Berja–Balanegra [125,137] and the 2000–2001 Albuñol series [139]. The main moderate historical earthquake close to the Campo de Dalías was the 1910 Adra earthquake (Figure 4) [126,140].

Intermediate seismicity is located southwest of the Granada Basin [141], mainly south of Málaga (Figure 3). It is mainly located at a depth between 30 km and 70 km, and the seismic zone strikes NE–SW on land and N–S on the coast and in the sea [142]. Deep earthquakes also occur, located in the SW of Sierra Nevada at a depth of over 600 km [143].

4.2.2. Earthquake Focal Mechanism Data and Current Stress Tensors

Earthquake focal mechanisms are highly varied (Figure 4). For small earthquakes, moment tensors with normal, reverse, and strike-slip kinematics can be found [43,113,144–146]. This variety has been associated with a complex crustal structure and local permutation of stresses [43]. The Granada Basin is characterized by NW–SE normal faulting earthquakes, as evidenced by the 1984 earthquake and the 2021 seismic series (Figure 4) [43,124,127]. This sector is also characterized by focal mechanism solutions with NW–SE to N–S low-angle nodal planes [104]. The Campo de Dalías and the adjacent Alboran Sea, on the contrary, are characterized by strike-slip faulting (Figure 4) [110,125,126].

The reduced stress tensor (Figure 4) of shallow seismicity reveals a vertical σ_1 and a NE–SW horizontal σ_3 in the eastern Granada Basin. In the central sector of the Granada Basin, the right dihedra diagrams of the 1988 Agrón series indicate two deformation phases [43]. One is related to a vertical P-axis and radial extension, while the other is related to a NW–SE horizontal P-axis and a NE–SW horizontal T-axis. In the western Granada Basin, the right dihedra diagrams show a P-axis that is almost vertical [44]. The diagram obtained from Vidal [144] displays a high dipping NW–SE P-axis and a predominantly NE–SW horizontal T-axis. The other diagram [146] shows an almost vertical P-axis, but it slightly dips to the ENE and mainly shows radial extension. In the Campo de Dalías and northern Alboran Sea, the P-axis is oriented horizontally NW–SE, while the T-axis is horizontal in the NE–SW direction [38].

The intermediate seismicity is mainly related to strike-slip and reverse faulting [142]. Ruiz Constán et al. [88] calculated two reduced stress tensors and right dihedra diagrams for earthquakes of the external arc of the slab and for earthquakes of the internal arc. The first group is related to a NW-inclined σ_1 and P-axis and SE-inclined σ_3 and T-axes. In the internal arc, both the reduced stress tensor and right dihedra diagram indicate the opposite.

4.3. GNSS Data

All the collected GNSS data show a W–SW-striking motion of the Betic Cordillera with respect to stable Eurasia plate (Figure 1) [31,34,93,147]. However, this motion is not uniform, as evidenced by the recently published local network data in the central Betic Cordillera [101,132,133,148].

The velocity vectors with respect to the stable Sierra Nevada (NEVA geodetic site) provide a clearer visualization of this motion (Figure 5). The 6200 and 6300 sites, located in the northern part of the Granada Basin, recorded S–SE-strike rates of 1.6 and 0.5 mm/year, respectively. The PAD and 6100 sites, located in the southern part of the Granada Basin, indicated motion to the SW at rates of 0.8 and 1.3 mm/year, respectively. The LOJA and 6000 stations, situated to the west of the Granada Basin, exhibited a WSW motion at rates of 0.7 and 0.6 mm/year, respectively. The MALA and PALM sites recorded SSW motion, with rates of 0.7 and 1.4 mm/year, respectively. Finally, the motion in Campo de Dalías is more complex. The 960 and 940 sites located in the Alpujárride Complex recorded southward motion at rates of 1.8 mm/year and 1.2 mm/year, respectively. The 990 and 970 sites

recorded northward motion; the 990 site to the NW showed a rate of 0.6 mm/year, and the 970 site to the NE showed a rate of 1.6 mm/year.

5. Discussion

5.1. Main Active Structures of the Central Betic Cordillera

The deformations and stresses in the study area are heterogeneous, although an extension striking NE–SW predominates, as indicated by structural, seismological, and geodetic data. In the eastern Granada Basin (Figure 2), the main structures are well-known NW–SE normal faults, such as the Granada Fault, the Padul Fault, and the Sierra Elvira faults [47,104,135]. NE–SW active faults, such as the Huenes Fault and the NE–SW faults of the Sierra Elvira, are also common [46]. These faults are mostly active strike-slip faults that are sinistral if they dip to NW and dextral if they dip to the SE [27]. These main structures accommodate the NE–SW extension of the sector, in agreement with the latest paleostresses (Figures 2 and 3) and current stresses (Figure 4). These data are consistent with W and SW motion obtained from the GNSS sites LOJA, 6100, PAD, and PALM (Figure 5). The NE–SW faults also present an important normal behaviour that could accommodate the NW–SE extension, and their activity is also in agreement with local radial extension in the area [42,43,119], as it happens in the present-day stresses of the 1988 Agrón seismic series (Figure 4). In fact, the activity of the ENE–WSW normal faults, such as the Tocón-Obeilár and Obeilár–Pinos Puente Faults [27,135], can explain the local southward displacement of site 6200, located in the hanging wall block of these faults.

GNSS data of the northern border of the Granada Basin indicate that this sector is currently moving to the W–SW with respect to stable Eurasia plate (Figure 1) [133], the most affected sector by strike-slip faulting (Figure 4). Similar observations have been made in the northern part of Sierra Gorda, where the 1998 Iznájar series indicated the activity of dextral strike-slip faults [108,109]. At the same time, the S–SE displacements with respect to stable NEVA, shown by the 6200 and 6300 sites (Figure 5), together with stress ellipsoid from striated pebbles [149], point locally to a recent NW–SE compression. Additionally, the ENE–WSW normal faults limiting the Granada Basin to the north were active until recent times [37] but may be locally inactive at present. This area could be suffering the permutation of horizontal NW–SE shortening related to Eurasia–Nubia convergence and the activity of normal dextral faults. The successive change of extension and compression in the same trend is common in the region, as evidenced by the analysis of stresses in the 1988 Agrón series [35].

The W and SW boundaries of the Granada Basin seem to be under compression and shortening, as evidenced by both recent faulting and GNSS data (Figures 2, 3 and 5). To the west, the N–S thrusts of the Sierra Gorda were active at least until the Tortonian, and the latest paleostress data suggest E–W compression perpendicular to main thrusts (Figures 2 and 3) [17]. At present, the shortening between the 6100 GNSS site with respect to the LOJA and 6000 sites suggests that contraction continues (Figure 5). To the southwest, deformation between the 6100 and MALA sites likewise indicate shortening in NE–SW direction (Figure 5), which could be related to an active development of the Sierra Tejeda antiform, further indicated by very incised drainage systems [37]. The reverse paleostresses align with the fold axis and suggest recent E–W and NE–SW compression. Both active and recent normal faulting is very common in the area (Figures 2–4) [145]. The Zafarraya Fault is the main active fault, presenting an E–W orientation associated with local N–S extension [134]. Despite this, it has been linked to compressional structures [35,37]. Active shortening may suggest that normal faulting is related to local structures resulting from the collapse of previously uplifted areas.

In the south of Sierra Nevada area, the latest paleostress analyses indicate simultaneous NNW–SSE and ENE–WSW extensions, with both normal and strike-slip faulting (Figures 2 and 3). The NNW–SSE extension aligns with the southward velocity rates recorded at GNNS sites 940 and 960, located in the northern sector of Campo de Dalías with respect to the Sierra Nevada (Figure 5). E–W folds forming the Sierra de Lújar and Sierra

de Gádor are the main structures in the area. However, E–W normal to normal–dextral faults are frequently observed in the Alpujarras Corridor [135,136,150,151], which must be active and explain the southward displacements. However, in the Campo de Dalías and the northern Alboran Sea, a new shortening front is occurring, where ENE–WSW active folding accommodates northward velocity rates measured at GNNS sites 990 and 970 (Figure 5) [101], in agreement with the NW–SE horizontal P-axis of earthquake focal mechanism solutions (Figure 4) [38]. Meanwhile, on the coast and offshore, dextral to normal faults, e.g., the Adra Fault, the Balangera Fault, and the Loma del Viento Fault, accommodate both NW–SE compression and NE–SW extension, also indicated by the T-axis of the known earthquake focal mechanisms (Figure 4) [38,110,112,140].

Most of the main active structures of the central Betic Cordillera do not affect the Nevado–Filábride complex [106], and the former complex is hardly affected by seismicity [33]. Therefore, these active structures are likely rooted at the Nevado Filábride–Alpujárride crustal detachment [24,104,106], named the Mecina detachment [20]. Ruano et al. [37] suggested that compressional structures of the western Granada Basin are also rooted in this detachment. The Mecina detachment was active during the Miocene [152], producing the a-type dome of the Sierra Nevada [22,62], and is probably still active at depth, as the Granada detachment is [104,106].

5.2. Extensional Collapse in the Central Betic Cordillera

Several models have been proposed to explain the extension in the central Betic Cordillera. On the one hand, it is understood as arc-parallel extension resulting from NW–SE convergence between Eurasia–Nubia [72,74,145], and uplift would derive from the formation of large E–W folds [24,35,59]. If so, the extension would be homogeneous NE–SW, orthogonal to the compression (Figure 5). In addition, a back-arc extension due to rollback has been suggested [31,34]. Considering that the subduction is related to the westward movement of the arc, the extension would be E–W. These two models alone do not explain the heterogeneous character of the extension suggested by the data. On the other hand, it has been proposed that it could be the result of the subducting slab-tearing W of the Granada Basin [81,153,154]. In this case, slab tearing would be responsible for the uplift of the Sierra Nevada with respect to a subsided area in the Alboran Sea, but not directly for the extension.

Following this line, the data presented here support the displacement from high-elevation zones surrounding the Sierra Nevada to more subsiding areas in the Western Alboran Basin, with a trend ranging from WSW in the Granada Basin to SSW to the south of the Sierra Nevada (Figure 6a). This trend and the structural data may indicate the extensional collapse of the upper levels of the crust in a WSW to S direction over the Mecina detachment in order to balance lateral contrasts in crustal thickness [136]. The uplift of the Nevado–Filábride Complex due to the overthickened crust related to westward ongoing slab tearing [81,88], denudation processes [155], and/or folding and thrusting [24,57,156] may have activated the Miocene extensional detachments in the W and SW of Sierra Nevada, which is also supported by geomorphological data [157]. Additionally, the active subduction with rollback located in the western Betic Cordillera [34,80,88] has produced subsidence and crustal thinning in the western and northern Alboran basins [54,158,159], facilitating the west–southwest–southwards collapse. However, the influence of both arc-parallel extension and back-arc extension due to rollback cannot be ruled out, as the ENE–WSW extension is the predominant.

The role of inherited structures of the Miocene evolution is important in the active gravitational collapse. In fact, the ENE–WSW to NE–SW extension is documented since the middle Miocene in the Granada Basin (Figure 6b) [27], and it is driven over the extensional detachment that exhumed the Nevado Filabride complex [20,104,106]. The activity of dextral faults extends up to Late Miocene in the Alpujarras Corridor located in the south of the Sierra Nevada [64]. The current activity of the western Alpujarras Corridor has also been suggested [113,160] and related to a Subduction-Transform Edge Propagator

fault [161]. However, the mainly southward displacement with respect to the Sierra Nevada (NEVA) of the GNNS sites PALM, 960, and 940 (Figure 5) suggests that at present, the Alpujarras Corridor is dominated by a N–S extension, in agreement with the activity of E–W normal and normal–dextral faults, such as the Laujar de Andarax and Ugíjar Faults (Figure 6c) [136,150,151].
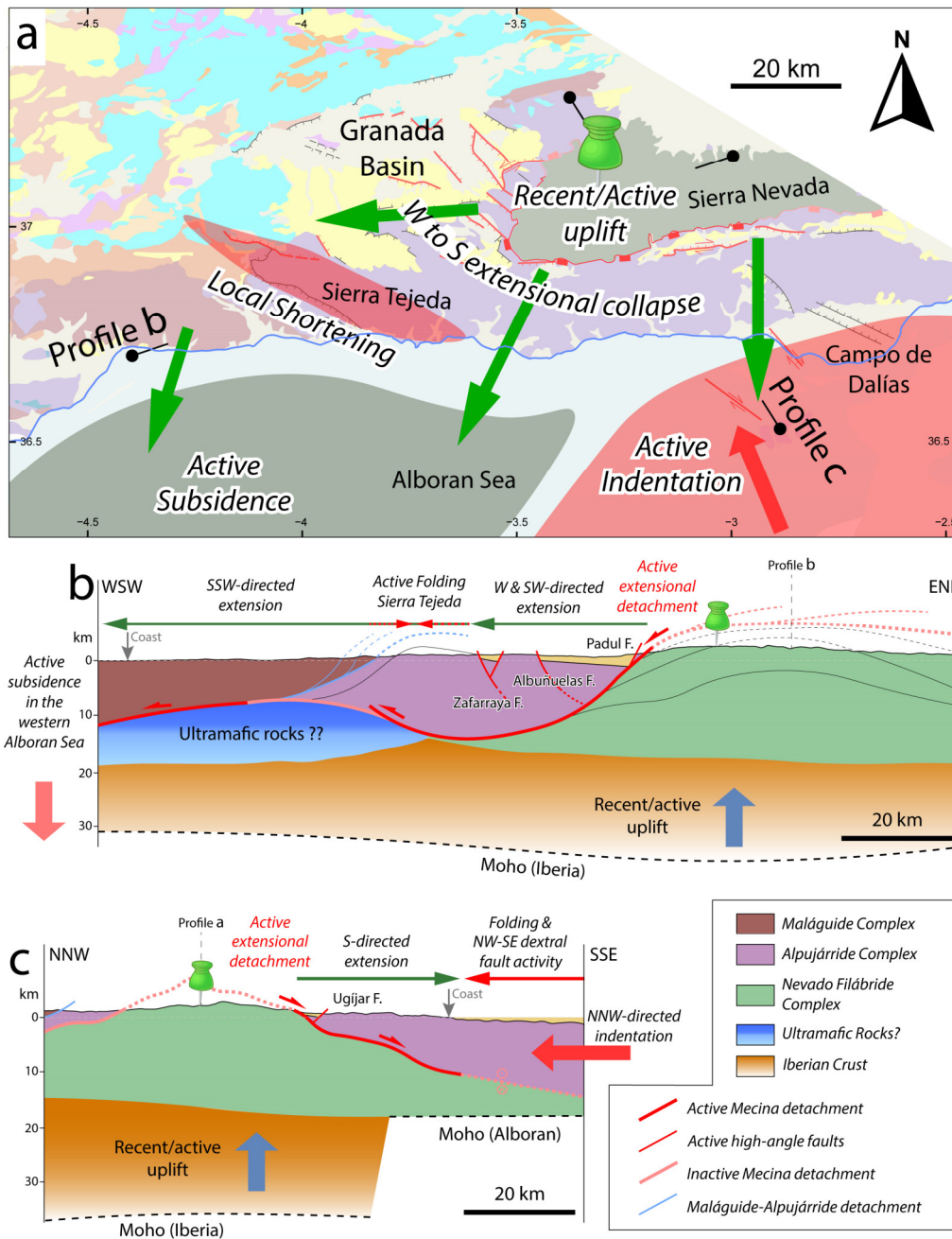

Figure 6. Simplified tectonic model of the central Betic Cordillera considering the Sierra Nevada (GNNS NEVA site) stable, indicated by a pushpin. (**a**) Extensional collapse in the central Betic Cordillera. Location of the (**b,c**) cross sections. (**b**) ENE–WSW profile from the Sierra Nevada, crossing the Granada Basin to the coast line of the western Alboran Sea. Crustal heterogeneities produce local shortening around the Sierra Tejeda. The upper crust model was modified from Bessiere et al. [162]. The Moho was taken from Barranco et al. [163]. The upper limit of ultramafic

rocks was taken from Barranco et al. [163] and Banda et al. [164]. (**c**) NNW–SSE profile from the South Iberian Domain, crossing the Sierra Nevada to the eastern Alboran Sea coast. Interaction between southward-directed extension over the Mecina detachment and indentation tectonics in the Alboran Sea produce folding and strike-slip faulting in the Alboran Sea coast. Moho depth was taken from Barranco et al. [163] and Galindo-Zaldívar et al. [156]. The geometry of the Mecina detachment was taken from Jabaloy et al. [152] and Marín-Lechado et al. [24].

The latest paleostresses determined in the W and SW of the Granada Basin suggest local E–W and NE–SW compression and align with the shortening observed by GNSS data. Reverse faulting is parallel to the Miocene thrusting in Sierra Gorda and perpendicular to the active shortening in the southern Sierra Gorda and the Sierra Tejeda [37]. This compressional front does not represent a fixed boundary of the collapse and only dumps locally the extensional collapse, as the GNNS MALA station continues to record an S–SW motion relative to a stable NEVA one (Figure 6a). The crustal heterogeneities [165] could be responsible for the development of this compressional front. Meanwhile, active indentation tectonics have affected the Alboran Sea [36,166,167], reaching the Iberian coast [101]. The compressions due to the active indentor form a fixed boundary and stop the southward directed collapse, producing well-developed E–W to ENE–WSW folds onshore and offshore in the Campo de Dalías (Figure 6b) [24]. Finally, the northern border of the Sierra Nevada appears to be inactive [157], and GNSS data indicate that it may be affected by shortening (Figure 5). Actually, the shallow extension is not as important to the north, in the South Iberian domain. Although it has been an area affected by arc-parallel extension [72–74,145,168], recent tectonic data do not suggest that this region is affected by stretching [30]. Moreover, seismicity is only found locally at the basement of the mountain front and the Guadalquivir Basin foreland [100,169,170] and in the southernmost part, in the Granada Basin [30,135]. On the other hand, the collapse from the Sierra Nevada onto the South Iberian domain is probably not as important as that in the south because the crust is already thickened towards the north [57,153].

In short, our data support a terminal subduction model of Iberian lithosphere beneath the Alboran Domain [79,80,82,84,85], producing rollback and subsidence in the Western Alboran Basin and uplift in the central Betic Cordillera. The latter is also affected by a NW–SE compression due to the Eurasia–Nubia convergence [28,171]. This framework leads to the extensional collapse from the Sierra Nevada towards the western Alboran Sea.

In the Betic Cordillera and likely further Mediterranean arcs, such as the Calabrian and the Hellenic Arcs, extensional collapse processes are ongoing, as recorded in relation to different orogenies throughout geological history. Examples include the Appalachian [172] and Western Gneiss Region, Norway [173] during the Paleozoic, and the Basin and Range Province (western United States and northwestern Mexico) during the Cretaceous [3,10,11]. The Mediterranean arcuate orogens are characterized by simultaneous thickening and thinning processes occurring in close proximity, leading to a synorogenic extensional collapse unlike the most prominent example of active postorogenic gravitational collapse occurring in the Tibetan Plateau [6,7,9]. All of these orogens have experienced similar Neogene–Quaternary evolution comprising the following tectonic processes [162]. On one hand, the crustal thickening, through either fold and thrust formation related to the Eurasia–Nubia convergence and/or slab tearing of previously subducting slabs [57,62,81,174], generate thicker crust. On the other hand, recent and active subduction with rollback [34,175–179] are derived in the formation of back-arc basins in the inner part of the arcs [12,180], resulting in a thinner crust. In contrast to the Tibetan Plateau, where the collapse affects the whole crust [8], the activity of normal detachment inherited form the Miocene evolution is currently dismantling the upper crust in a general context of active shortening, at least in the Betic Cordillera [28,171]. In summary, the active extension in the central Betic Cordillera in a context of generalized thickening and plate convergence represents a good example of extensional collapse for the Mediterranean region and worldwide, because localized thinning processes due to terminal subduction and the arcuate shape of the orogens enhance the collapse of the uplifted regions.

6. Conclusions

The present-day development of the seismically active Granada Basin and the surrounding areas is a consequence of the extensional collapse of the central Betic Cordillera in the frame of the Eurasia–Nubia plate convergence. The combination of structural geologic, seismologic, and geodetic data allow the constraining of the active deformation of the basin and surrounding region that accommodated the heterogeneous extension.

The Sierra Nevada, the main antiformal structure affecting the metamorphic basement of the Alboran Domain, has become a relative stable and aseismic and is the most elevated metamorphic massif in the Cordillera. The E–W to NE–SW extension in the W–SW of the Sierra Nevada accommodated by the extensional system of the Granada Basin, together with the southward displacement to the S of the Sierra Nevada, suggest an active extensional collapse of the shallow crustal levels over the Mecina detachment.

Two boundaries constrain the collapse to the W–SW and S: (a) a near to fixed boundary located to the W and SW of the Granada Basin, made up by active N–S to WNW–ESE thrust and folds and formed due to crustal heterogeneities; (b) a fixed boundary located in the Campo de Dalías that has undergone both NE–SW extension and NW–SE compression related to the active indentation in the Alboran Basin and accommodated by ENE–WSW folds and NW–SE normal and dextral faults.

The upper crustal extensional collapse is probably driven by typical processes affecting the Mediterranean orogenic arcs: (a) overthickening that uplift the central sector of the Betic Cordillera and (b) back-arc crustal thinning and ongoing supra-subduction subsidence in the western and central Alboran Sea.

References

1. Rey, P.F.; Vanderhaeghe, O.; Teyssier, C. Gravitational Collapse of the Continental Crust: Definition, Regimes and Modes. *Tectonophysics* **2001**, *342*, 435–449. [CrossRef]
2. Van Bemmelen, R.W. Principles of Mountain Building. In *Mountain Building: A Study Primarily Based on Indonesia Region of the World's Most Active Crustal Deformations*; Springer: Dordrecht, The Netherlands, 1954; pp. 1–34.
3. Dewey, J.F. Extensional Collapse of Orogens. *Tectonics* **1988**, *7*, 1123–1139. [CrossRef]
4. Foster, D.A.; Ma, C.; Goscombe, B.D.; Mueller, P.A. Extensional Collapse of Orogens: A Review and Example from the Southern Appalachian Orogen. *Compressional Tecton. Plate Converg. Mt. Build.* **2023**, *1*, 301–319.
5. Burchfiel, B.C.; Royden, L.H. North-South Extension within the Convergent Himalayan Region. *Geology* **1985**, *13*, 679–682. [CrossRef]
6. England, P.C.; Houseman, G.A. The Mechanics of the Tibetan Plateau. *Philos. Trans. R. Soc. London. Ser. A Math. Phys. Sci.* **1988**, *326*, 301–320.
7. England, P.C.; Houseman, G.A. Extension during Continental Convergence, with Application to the Tibetan Plateau. *J. Geophys. Res.* **1989**, *94*, 17561–17579. [CrossRef]
8. Liu, M.; Yaung, Y. Extensional Collapse of the Tibetan Plateau: Results of Three-Dimensional Finite Element Modeling. *J. Geophys. Res.* **2003**, *108*, 2361. [CrossRef]
9. Kellett, D.A.; Cottle, J.M.; Larson, K.P. The South Tibetan Detachment System: History, Advances, Definition and Future Directions. *Geol. Soc. Spec. Publ.* **2019**, *483*, 377–400. [CrossRef]
10. Jones, C.H.; Unruht, J.R.; Sonder, L.J. The Role of Gravitational Potential Energy in Active Deformation in the Southwestern United States. *Nature* **1996**, *381*, 37–41. [CrossRef]
11. Flesch, L.M.; Holt, W.E.; Haines, A.J.; Shen-Tu, B. Dynamics of the Pacific-North American Plate Boundary in the Western United States. *Science* **2000**, *287*, 834–836. [CrossRef]
12. Van Hinsbergen, D.J.J.; Vissers, R.L.M.; Spakman, W. Origin and Consequences of Western Mediterranean Subduction, Rollback, and Slab Segmentation. *Tectonics* **2014**, *33*, 393–419. [CrossRef]
13. Leprêtre, R.; De Lamotte, D.F.; Combier, V.; Gimeno-Vives, O.; Mohn, G.; Eschard, R. The Tell-Rif Orogenic System (Morocco, Algeria, Tunisia) and the Structural Heritage of the Southern Tethys Margin. *BSGF-Earth Sci. Bull.* **2018**, *189*, 10.
14. Platt, J.; Vissers, R. Extensional Collapse of Thickened Continental Lithosphere: A Working Hypothesis for the Alboran Sea and Gibraltar Arc. *Geology* **1989**, *17*, 540–543. [CrossRef]
15. García-Dueñas, V.; Balanyá, J.; Martínez-Martínez, J. Miocene Extensional Detachments in the Outcropping Basement of the Northern Alboran Basin (Betics) and Their Tectonic Implications. *Geo-Mar. Lett.* **1992**, *12*, 88–95. [CrossRef]
16. Balanyá, J.C.; García-Dueñas, V.; Azañón, J.M.; Sánchez-Gómez, M. Alternating Contractional and Extensional Events in the Alpujarride Nappes of the Alboran Domain (Betics, Gibraltar Arc). *Tectonics* **1997**, *16*, 226–238. [CrossRef]
17. Galindo-Zaldívar, J.; Ruano, P.; Jabaloy, A.; López-Chicano, M. Kinematics of Faults between Subbetic Units during the Miocene (Central Sector of the Betic Cordillera). *Comptes Rendus L'Acad. Sci. Ser. IIA-Earth Planet. Sci.* **2000**, *331*, 811–816. [CrossRef]
18. Platt, J.; Behr, W.; Johanesen, K.; Williams, J. The Betic-Rif Arc and Its Orogenic Hinterland: A Review. *Annu. Rev. Earth Planet. Sci.* **2013**, *41*, 313–357. [CrossRef]
19. López Sánchez-Vizcaíno, V.; Rubatto, D.; Gómez-Pugnaire, M.; Trommsdorff, V. Middle Miocene High-Pressure Metamorphism and Fast Exhumation of the Nevado-Filábride Complex, SE Spain. *Terra Nova* **2001**, *13*, 327–332. [CrossRef]
20. Galindo-Zaldívar, J.; González-Lodeiro, F.; Jabaloy, A. Structures Progressives En Cisaillement Extensif Dans Un Detachement a La Partie Occidentale de La Sierra Nevada (Cordilleres Betiques, Espagne). *Geodin. Acta* **1989**, *3*, 73–85. [CrossRef]
21. Jabaloy, A.; Galindo-Zaldívar, J.; González-Lodeiro, F. The Mecina Extensional System: Its Relation with the Post-Aquitanian Piggy-Back Basins and the Paleostresses Evolution (Betic Cordilleras, Spain). *Geo-Mar. Lett.* **1992**, *12*, 96–103. [CrossRef]
22. Martínez-Martínez, J.M.; Soto, J.I.; Balanyá, J.C. Orthogonal Folding of Extensional Detachments: Structure and Origin of the Sierra Nevada Elongated Dome (Betics, SE Spain). *Tectonics* **2002**, *21*, 3-1–3-20. [CrossRef]
23. Sanz de Galdeano, C. Geologic Evolution of the Betic Cordilleras in the Western Mediterranean, Miocene to the Present. *Tecfonophysics* **1990**, *172*, 107–119. [CrossRef]
24. Marín-Lechado, C.; Galindo-Zaldívar, J.; Rodríguez-Fernández, L.R.; Pedrera, A. Mountain Front Development by Folding and Crustal Thickening in the Internal Zone of the Betic Cordillera-Alboran Sea Boundary. *Pure Appl. Geophys.* **2007**, *164*, 1–21. [CrossRef]
25. Augier, R.; Jolivet, L.; Robin, C. Late Orogenic Doming in the Eastern Betic Cordilleras: Final Exhumation of the Nevado-Filabride Complex and Its Relation to Basin Genesis. *Tectonics* **2005**, *24*, TC4003. [CrossRef]
26. Augier, R.; Agard, P.; Monié, P.; Jolivet, L.; Robin, C.; Booth-Rea, G. Exhumation, Doming and Slab Retreat in the Betic Cordillera (SE Spain): In Situ 40Ar/39 AR Ages and P-T-d-t Paths for the Nevado-Filabride Complex. *J. Metamorph. Geol.* **2005**, *23*, 357–381. [CrossRef]
27. Rodríguez-Fernández, J.; Sanz de Galdeano, C. Late Orogenic Intramontane Basin Development: The Granada Basin, Betics (Southern Spain). *Basin Res.* **2006**, *18*, 85–102. [CrossRef]
28. DeMets, C.; Gordon, R.G.; Argus, D.F. Geologically Current Plate Motions. *Geophys. J. Int.* **2010**, *181*, 1–80. [CrossRef]
29. Stich, D.; Serpelloni, E.; de Lis Mancilla, F.; Morales, J. Kinematics of the Iberia-Maghreb Plate Contact from Seismic Moment Tensors and GPS Observations. *Tectonophysics* **2006**, *426*, 295–317. [CrossRef]

30. Palano, M.; González, P.J.; Fernández, J. The Diffuse Plate Boundary of Nubia and Iberia in the Western Mediterranean: Crustal Deformation Evidence for Viscous Coupling and Fragmented Lithosphere. *Earth Planet. Sci. Lett.* **2015**, *430*, 439–447. [CrossRef]

31. Galindo-Zaldívar, J.; Gil, A.J.; Sanz de Galdeano, C.; Lacy, M.C.; García-Armenteros, J.A.; Ruano, P.; Ruiz-Armenteros, A.M.; Martínez-Martos, M.; Alfaro, P. Active Shallow Extension in Central and Eastern Betic Cordillera from CGPS Data. *Tectonophysics* **2015**, *663*, 290–301. [CrossRef]

32. Sparacino, F.; Palano, M.; Peláez, J.A.; Fernández, J. Geodetic Deformation versus Seismic Crustal Moment-Rates: Insights from the Ibero-Maghrebian Region. *Remote Sens.* **2020**, *12*, 952. [CrossRef]

33. IGN Earthquake Catalogue. Available online: https://www.ign.es/web/ign/portal/sis-catalogo-terremotos/ (accessed on 30 May 2023).

34. González-Castillo, L.; Galindo-Zaldivar, J.; de Lacy, M.C.; Borque, M.J.; Martinez-Moreno, F.J.; García-Armenteros, J.A.; Gil, A.J. Active Rollback in the Gibraltar Arc: Evidences from CGPS Data in the Western Betic Cordillera. *Tectonophysics* **2015**, *663*, 310–321. [CrossRef]

35. Galindo-Zaldívar, J.; Gil, A.; Borque, M.; González-Lodeiro, F.; Jabaloy, A.; Marín-Lechado, C.; Ruano, P.; Sanz de Galdeano, C. Active Faulting in the Internal Zones of the Central Betic Cordilleras (SE, Spain). *J. Geodyn.* **2003**, *36*, 239–250. [CrossRef]

36. Estrada, F.; Galindo-Zaldívar, J.; Vázquez, J.T.; Ercilla, G.; D'Acremont, E.; Alonso, B.; Gorini, C. Tectonic Indentation in the Central Alboran Sea (Westernmost Mediterranean). *Terra Nova* **2018**, *30*, 24–33. [CrossRef]

37. Ruano, P.; Galindo-Zaldívar, J.; Jabaloy, A. Recent Tectonic Structures in a Transect of the Central Betic Cordillera. *Pure Appl. Geophys.* **2004**, *161*, 541–563. [CrossRef]

38. Marín-Lechado, C.; Galindo-Zaldívar, J.; Rodríguez-Fernández, L.R.; Serrano, I.; Pedrera, A. Active Faults, Seismicity and Stresses in an Internal Boundary of a Tectonic Arc (Campo de Dalías and Níjar, Southeastern Betic Cordilleras, Spain). *Tectonophysics* **2005**, *396*, 81–96. [CrossRef]

39. Rodríguez Fernández, L.R.; López Olmedo, F.; Oliveira, J.T.; Medialdea, T.; Terrinha, P.; Matas, J.; Martín-Serrano, A.; Martín Parra, L.M.; Rubio, F.; Marín, C.; et al. *Mapa Geológico de La Península Ibérica, Baleares y Canarias a Escala 1:1,000,000*; IGME: Madrid, Spain, 2015.

40. García-Mayordomo, J.; Martín-Banda, R. Guide for the Use of QAFI v.4. Available online: http://info.igme.es/qafi/ (accessed on 30 May 2023).

41. López-Chicano, M. Contribución al Conocimiento Del Sistema Hidrogeológico Kárstico de Sierra Gorda y Su Entorno (Granada y Málaga). Ph.D. Thesis, University of Granada, Granada, Spain, 1992.

42. Galindo-Zaldívar, J.; González-Lodeiro, F.; Jabaloy, A. Stress and Palaeostress in the Betic-Rif Cordilleras (Miocene to the Present). *Tectonophysics* **1993**, *227*, 105–126. [CrossRef]

43. Galindo-Zaldívar, J.; Jabaloy, A.; Serrano, I.; Morales, J.; González-Lodeiro, F.; Torcal, F. Recent and Present-Day Stresses in the Granada Basin (Betic Cordilleras)' Example of a Late Miocene-Present-Day Extensional Basin in a Convergent Plate Boundary. *Tectonics* **1999**, *18*, 686–702. [CrossRef]

44. Ruano, P. Estructuras Tectónicas Recientes En La Transversal Central de Las Cordilleras Béticas. Ph.D. Thesis, University of Granada, Granada, Spain, 2003.

45. Marín Lechado, C. Estructura y Evolución Tectónica Reciente Del Campo de Dalías y de Níjar En El Contexto Del Límite Meridional de Las Cordilleras Béticas Orientales. Ph.D. Thesis, University of Granada, Granada, Spain, 2005.

46. Reicherter, K.R.; Peters, G. Neotectonic Evolution of the Central Betic Cordilleras (Southern Spain). *Tectonophysics* **2005**, *405*, 191–212. [CrossRef]

47. Sanz de Galdeano, C.; García-Tortosa, F.; Peláez, J.A.; Alfaro, P.; Azañón, J.M.; Galindo-Zaldívar, J.; Lopéz Casado, C.; López Garrido, A.; Rodríguez-Fernández, J.; Ruano, P. Main Active Faults in the Granada and Guadix-Baza Basins (Betic Cordillera). *J. Iber. Geol.* **2012**, *38*, 209–223. [CrossRef]

48. Fontboté, J.M.; Estévez, A. Geología de Las Cordilleras Béticas. *Bol. Geol. Min.* **1980**, *91*, 249–292.

49. García-Hernández, M.; López-Garrido, A.C.; Rivas, P.; Sanz de Galdeano, C.; Vera, J.A. Mesozoic Palaeogeographic Evolution of the External Zones of the Betic Cordillera. *Geol. Mijnb.* **1980**, *59*, 155–168.

50. Lonergan, L.; White, N. Origin of the Betic-Rif Mountain Belt. *Tectonics* **1997**, *16*, 504–522. [CrossRef]

51. Meijninger, B.; Vissers, R. Thrust-Related Extension in the Prebetic (Southern Spain) and Clousure of the North Betic Strait. *Rev. Soc. Geol. Esp.* **2007**, *20*, 153–171.

52. Fallot, P. Les Cordilléres Betiques. *Estud. Geol.* **1948**, *4*, 259–279.

53. Tubía, J.M.; Cuevas, J.; Gil Ibarguchi, J.I. Sequential Development of the Metamorphic Aureole beneath the Ronda Peridotites and Its Bearing on the Tectonic Evolution of the Betic Cordillera. *Tectonophysics* **1997**, *279*, 227–252. [CrossRef]

54. Do Couto, D.; Gorini, C.; Jolivet, L.; Lebret, N.; Augier, R.; Gumiaux, C.; d'Acremont, E.; Ammar, A.; Jabour, H.; Auxietre, J.L. Tectonic and Stratigraphic Evolution of the Western Alboran Sea Basin in the Last 25 Myrs. *Tectonophysics* **2016**, *677–678*, 280–311. [CrossRef]

55. Sala, M. Baetic Cordillera and Guadalquivir Basin. In *Geomorphology of Europe*; Palgrave: London, UK, 1984; pp. 323–340.

56. Sanz de Galdeano, C.; Vera, J.A. Stratigraphic Record and Palaeogeographical Context of the Neogene Basins in the Betic Cordillera, Spain. *Basin Res.* **1992**, *4*, 21–36. [CrossRef]

57. Pedrera, A.; Ruiz-Constán, A.; García-Senz, J.; Azor, A.; Marín-Lechado, C.; Ayala, C.; Díaz de Neira, J.A.; Rodríguez-Fernández, L.R. Evolution of the South-Iberian Paleomargin: From Hyperextension to Continental Subduction. *J. Struct. Geol.* **2020**, *138*, 104122. [CrossRef]

58. Braga, J.C.; Martín, J.; Quesada, C. Patterns and Average Rates of Late Neogene- Recent Uplift of the Betic Cordillera, SE Spain. *Geomorphology* **2003**, *50*, 3–26. [CrossRef]

59. Sanz de Galdeano, C.; Alfaro, P. Tectonic Significance of the Present Relief of the Betic Cordillera. *Geomorphology* **2004**, *63*, 175–190. [CrossRef]

60. Aldaya, F.; Álvarez, F.; Galindo-Zaldívar, J.; González-Lodeiro, F.; Jabaloy, A.; Navarro-Vilá, F. The Maláguide-Alpujárride Contact (Betic Cordilleras, Spain): A Brittle Extensional Detachment. *CR Acad. Sci. Paris* **1991**, *313*, 1447–1453.

61. Martínez-Martínez, J.M.; Azañón, J.M. Mode of Extensional Tectonics in the Southeastern Betics (SE Spain): Implications for the Tectonic Evolution of the Peri-Alborán Orogenic System. *Tectonics* **1997**, *16*, 205–225. [CrossRef]

62. Jolivet, L.; Famin, V.; Mehl, C.; Parra, T.; Aubourg, C.; Hébert, R.; Philippot, P. *Strain Localization during Crustal-Scale Boudinage to Form Extensional Metamorphic Domes in the Aegean Sea*; Special Papers; Geological Society of America: Boulder, CO, USA, 2004; pp. 185–210.

63. Le Pourhiet, L.; Huet, B.; May, D.A.; Labrousse, L.; Jolivet, L. Kinematic Interpretation of the 3D Shapes of Metamorphic Core Complexes. *Geochem. Geophys. Geosyst.* **2012**, *13*, Q09002. [CrossRef]

64. Sanz de Galdeano, C.; Rodríguez-Fernández, J.; López Garrido, Á.C. A Strike-Slip Fault Corridor within the Alpujarra Mountains (Betic Cordilleras, Spain). *Geol. Rundsch.* **1985**, *74*, 641–655. [CrossRef]

65. Lonergan, L.; Platt, J.P.; Gallagher, L. The Internal-External Zone Boundary in the Eastern Betic Cordillera, SE Spain. *J. Struct. Geol.* **1994**, *16*, 175–188. [CrossRef]

66. Frasca, G.; Gueydan, F.; Brun, J.P.; Monié, P. Deformation Mechanisms in a Continental Rift up to Mantle Exhumation. Field Evidence from the Western Betics, Spain. *Mar. Pet. Geol.* **2016**, *76*, 310–328. [CrossRef]

67. Crespo-Blanc, A.; Frizon, D.; Lamotte, D.E. Structural Evolution of the External Zones Derived from the Flysch Trough and the South Iberian and Maghrebian Paleomargins around the Gibraltar Arc: A Comparative Study. *Bull. Soc. Géol. Fr.* **2006**, *177*, 267–282. [CrossRef]

68. Crespo-Blanc, A. Superimposed Folding and Oblique Structures in the Palaeomargin-Derived Units of the Central Betics (SW Spain). *J. Geol. Soc. Lond.* **2007**, *164*, 621–636. [CrossRef]

69. Crespo-Blanc, A. Recess Drawn by the Internal Zone Outer Boundary and Oblique Structures in the Paleomargin-Derived Units (Subbetic Domain, Central Betics): An Analogue Modelling Approach. *J. Struct. Geol.* **2008**, *30*, 65–80. [CrossRef]

70. Sierro, F.J.; González-Delgado, J.A.; Dabrio, C.J.; Flores, J.A.; Civis, J. Late Neogene Depositional Sequences in the Foreland Basin of Guadalquivir (SW Spain). In *Tertiary Basins of Spain: The Stratigraphic Record of Crustal Kinematics*; Friend, P., Dabrio, C.J., Eds.; Cambridge Univ. Press: Cambridge, UK, 1996; pp. 339–345.

71. Azañón, J.M.; Roldán, F.J.; Rodríguez-Fernández, J. Fallas y Despegues Extensionales En El Subbético Central: Implicaciones En La Evolución Neógena de Las Zonas Externas de La Cordillera Bética. *Geogaceta* **2012**, *52*, 13–16.

72. Jimenez-Bonilla, A.; Torvela, T.; Balanyá, J.C.; Expósito, I.; Díaz-Azpiroz, M. Changes in Dip and Frictional Properties of the Basal Detachment Controlling Orogenic Wedge Propagation and Frontal Collapse: The External Central Betics Case. *Tectonics* **2016**, *35*, 3028–3049. [CrossRef]

73. Crespo-Blanc, A.; Comas, M.; Balanyá, J.C. Clues for a Tortonian Reconstruction of the Gibraltar Arc: Structural Pattern, Deformation Diachronism and Block Rotations. *Tectonophysics* **2016**, *683*, 308–324. [CrossRef]

74. Balanyá, J.C.; Crespo-Blanc, A.; Díaz Azpiroz, M.; Expósito, I.; Luján, M. Structural Trend Line Pattern and Strain Partitioning around the Gibraltar Arc Accretionary Wedge: Insights as to the Mode of Orogenic Arc Building. *Tectonics* **2007**, *26*, TC2005. [CrossRef]

75. Calvert, A.; Sandvol, E.; Seber, D.; Barazangi, M.; Vidal, F.; Alguacil, G.; Jabour, N. Propagation of Regional Seismic Phases (Lg and Sn) and Pn Velocity Structure along the Africa-Iberia Plate Boundary Zone: Tectonic Implications. *Geophys. J. Int.* **2000**, *142*, 384–408. [CrossRef]

76. Seber, D.; Barazangi, M.; Ibenbrahim, A.; Demnati, A. Geophysical Evidence for Lithospheric Delamination beneath the Alboran Sea and Rif-Betic Mountains. *Nature* **1996**, *379*, 785–790. [CrossRef]

77. Houseman, G.A.; McKenzie, D.P.; Molnar, P. Convective Instability of a Thickened Boundary Layer and Its Relevance for the Thermal Evolution of Continental Convergent Belts. *J. Geophys. Res.* **1981**, *86*, 6115–6132. [CrossRef]

78. Chertova, M.; Spakman, W.; Geenen, T.; van den Berg, A.; van Hinsbergen, D. Underpinning Tectonic Reconstructions of the Western Mediterranean Region with Dynamic Slab Evolution from 3-D Numerical Modeling. *J. Geophys. Res. Solid. Earth* **2014**, *119*, 3678–3699. [CrossRef]

79. Rosenbaum, G.; Lister, G.S.; Duboz, C. Reconstruction of the Tectonic Evolution of the Western Mediterranean since the Oligocene. *J. Virtual Explor.* **2002**, *8*, 107–130. [CrossRef]

80. Pedrera, A.; Ruiz-Constán, A.; Galindo-Zaldívar, J.; Chalouan, A.; Sanz de Galdeano, C.; Marín-Lechado, C.; Ruano, P.; Benmakhlouf, M.; Akil, M.; López-Garrido, A.C.; et al. Is There an Active Subduction beneath the Gibraltar Orogenic Arc? Constraints from Pliocene to Present-Day Stress Field. *J. Geodyn.* **2011**, *52*, 83–96. [CrossRef]

81. Mancilla, F.d.L.; Booth-Rea, G.; Stich, D.; Pérez-Peña, J.V.; Morales, J.; Azañón, J.M.; Martin, R.; Giaconia, F. Slab Rupture and Delamination under the Betics and Rif Constrained from Receiver Functions. *Tectonophysics* **2015**, *663*, 225–237. [CrossRef]

82. Spakman, W.; Wortel, R. A Tomographic View on Western Mediterranean Geodynamics. In *The TRANSMED Atlas. The Mediterranean Region from Crust to Mantle*; Springer: Berlin/Heidelberg, Germany, 2004; pp. 31–52.

83. Lacombe, O.; Romagny, A.; Jolivet, L.; Menant, A.; Bessière, E.; Maillard, A.; Canva, A.; Gorini, C.; Augier, R. Detailed Tectonic Reconstructions of the Western Mediterranean Region for the Last 35 Ma, Insights on Driving Mechanisms. *BSGF-Earth Sci. Bull.* **2020**, *191*, 37. [CrossRef]

84. Blanco, M.J.; Spakman, W. The P-Wave Velocity Structure of the Mantle below the Iberian Peninsula: Evidence for Subducted Lithosphere below Southern Spain. *Tectonophysics* **1993**, *221*, 13–34. [CrossRef]

85. Gill, R.C.O.; Aparicio, A.; El Azzouzi, M.; Hernandez, J.; Thirlwall, M.F.; Bourgois, J.; Marriner, G.F. Depleted Arc Volcanism in the Alboran Sea and Shoshonitic Volcanism in Morocco: Geochemical and Isotopic Constraints on Neogene Tectonic Processes. *Lithos* **2004**, *78*, 363–388. [CrossRef]

86. Hoernle, K.; van den Bogaard, P.; Duggen, S.; Mocek, B.; Garbe-Schonberg, D. Evidence for Miocene Subduction beneath the Alboran Sea: 40Ar/39Ar Dating and Geochemistry of Volcanic Rocks from Holes 977A and 978A. *Proc. Ocean. Drill. Program Sci. Results* **1999**, *161*, 357–373. [CrossRef]

87. Comas, M.C.; Platt, J.P.; Soto, J.I.; Watts, A.B. The Origin and Tectonic History of the Alboran Basin: Insights from Leg 161 Results. *Proc. Ocean. Drill. Program Sci. Results* **1999**, *161*, 555–580. [CrossRef]

88. Ruiz-Constán, A.; Galindo-Zaldívar, J.; Pedrera, A.; Célérier, B.; Marín-Lechado, C. Stress Distribution at the Transition from Subduction to Continental Collision (Northwestern and Central Betic Cordillera). *Geochem. Geophys. Geosyst.* **2011**, *12*, Q12002. [CrossRef]

89. Ruiz-Constán, A.; Pedrera, A.; Galindo-Zaldívar, J.; Pous, J.; Arzate, J.; Roldn-García, F.J.; Marin-Lechado, C.; Anahnah, F. Constraints on the Frontal Crustal Structure of a Continental Collision from an Integrated Geophysical Research: The Central-Western Betic Cordillera (SW Spain). *Geochem. Geophys. Geosyst.* **2012**, *13*, Q08012. [CrossRef]

90. Duggen, S.; Hoernle, K.; van den Bogaard, P.; Garbe-Schönberg, D. Post-Collisional Transition from Subduction-to Intraplate-Type Magmatism in the Westernmost Mediterranean: Evidence for Continental-Edge Delamination of Subcontinental Lithosphere. *J. Petrol.* **2005**, *46*, 1155–1201. [CrossRef]

91. Duggen, S.; Hoernle, K.; Klügel, A.; Geldmacher, J.; Thirlwall, M.; Hauff, F.; Lowry, D.; Oates, N. Geochemical Zonation of the Miocene Alborán Basin Volcanism (Westernmost Mediterranean): Geodynamic Implications. *Contrib. Mineral. Petrol.* **2008**, *156*, 577–593. [CrossRef]

92. Bezada, M.J.; Humphreys, E.D.; Toomey, D.R.; Harnafi, M.; Dávila, J.M.; Gallart, J. Evidence for Slab Rollback in Westernmost Mediterranean from Improved Upper Mantle Imaging. *Earth Planet. Sci. Lett.* **2013**, *368*, 51–60. [CrossRef]

93. Koulali, A.; Ouazar, D.; Tahayt, A.; King, R.W.; Vernant, P.; Reilinger, R.E.; McClusky, S.; Mourabit, T.; Davila, J.M.; Amraoui, N. New GPS Constraints on Active Deformation along the Africa-Iberia Plate Boundary. *Earth Planet. Sci. Lett.* **2011**, *308*, 211–217. [CrossRef]

94. González-Castillo, L.; Galindo-Zaldívar, J.; Pedrera, A.; Martínez-Moreno, F.J.; Ruano, P. Shallow Frontal Deformation Related to Active Continental Subduction: Structure and Recent Stresses in the Westernmost Betic Cordillera. *Terra Nova* **2015**, *27*, 114–121. [CrossRef]

95. Ruiz-Constán, A.; Stich, D.; Galindo-Zaldívar, J.; Morales, J. Is the Northwestern Betic Cordillera Mountain Front Active in the Context of the Convergent Eurasia-Africa Plate Boundary? *Terra Nova* **2009**, *21*, 352–359. [CrossRef]

96. Borque, M.J.; Sánchez-Alzola, A.; Martin-Rojas, I.; Alfaro, P.; Molina, S.; Rosa-Cintas, S.; Rodríguez-Caderot, G.; de Lacy, C.; García-Armenteros, J.A.; Avilés, M.; et al. How Much Nubia-Eurasia Convergence Is Accommodated by the NE End of the Eastern Betic Shear Zone (SE Spain)? Constraints From GPS Velocities. *Tectonics* **2019**, *38*, 1824–1839. [CrossRef]

97. Bousquet, J.C. Quaternary Strike-Slip Faults in Southeastern Spain. *Tectonophysics* **1979**, *52*, 277–286. [CrossRef]

98. Silva, P.G.; Goy, J.L.; Zazo, C.; Bardají, T. Faulth-Generated Mountain Fronts in Southeast Spain: Geomorphologic Assessment of Tectonic and Seismic Activity. *Geomorphology* **2003**, *50*, 203–225. [CrossRef]

99. Coppier, G.; Griveaud, P.; De Larouziere, F.D.; Montenat, C.; Ott d'estevou, P. Exemple de Poinronnement Tectonique Neogene Dans Les Cordilleres Betiques Orientales: L'Are d'Aguilas (Sud-Est de l'Espagne). *Geodin. Acta* **1989**, *3*, 37–51. [CrossRef]

100. Tendero-Salmerón, V.; Galindo-Zaldivar, J.; Peláez, J.A.; Martínez-Martos, M.; Henares, J.; Marín-Lechado, C.; Gil, A.J.; López-Garrido, Á.C. Seismicity in Strike-Slip Foreland Faults (Central Betic Cordillera Front): Evidence of Indentation Tectonics. *Tectonics* **2020**, *39*, e2020TC006143. [CrossRef]

101. Galindo-Zaldívar, J.; Gil, A.J.; Tendero-Salmerón, V.; Borque, M.J.; Ercilla, G.; González-Castillo, L.; Sánchez-Alzola, A.; Lacy, M.C.; Estrada, F.; Avilés, M.; et al. The Campo de Dalias GNSS Network Unveils the Interaction between Roll-Back and Indentation Tectonics in the Gibraltar Arc. *Sensors* **2022**, *22*, 2128. [CrossRef] [PubMed]

102. Medina-Cascales, I.; Koch, L.; Cardozo, N.; Martin-Rojas, I.; Alfaro, P.; García-Tortosa, F.J. 3D Geometry and Architecture of a Normal Fault Zone in Poorly Lithified Sediments: A Trench Study on a Strand of the Baza Fault, Central Betic Cordillera, South Spain. *J. Struct. Geol.* **2019**, *121*, 25–45. [CrossRef]

103. Sanz de Galdeano, C.; Shanov, S.; Galindo-Zaldívar, J.; Radulov, A.; Nikolov, G. A New Tectonic Discontinuity in the Betic Cordillera Deduced from Active Tectonics and Seismicity in the Tabernas Basin. *J. Geodyn.* **2010**, *50*, 57–66. [CrossRef]

104. Madarieta-Txurruka, A.; Galindo-Zaldívar, J.; González-Castillo, L.; Peláez, J.A.; Ruiz-Armenteros, A.M.; Henares, J.; Garrido-Carretero, M.S.; Avilés, M.; Gil, A.J. High- and Low-Angle Normal Fault Activity in a Collisional Orogen: The Northeastern Granada Basin (Betic Cordillera). *Tectonics* **2021**, *40*, e2021TC006715. [CrossRef]

105. Serpelloni, E.; Vannucci, G.; Pondrelli, S.; Argnani, A.; Casula, G.; Anzidei, M.; Baldi, P.; Gasperini, P. Kinematics of the Western Africa-Eurasia Plate Boundary from Focal Mechanisms and GPS Data. *Geophys. J. Int.* **2007**, *169*, 1180–1200. [CrossRef]
106. Galindo-Zaldívar, J.; Jabaloy, A.; González-Lodeiro, F. Reactivation Du Detachement Extensif de Mecina Dans Le Secteur Occidental de La Sierra Nevada (Cordilleres Betiques, SE de l'Espagne). *Comptes Rendus L'Acad. Sci. Ser. IIA-Sci. Terre Planetes* **1996**, *323*, 615–622.
107. Sanz de Galdeano, C. The Zafarraya Polje (Betic Cordillera, Granada, Spain), a Basin Open by Lateral Displacement and Bending. *J. Geodyn.* **2013**, *64*, 62–70. [CrossRef]
108. Carmona, E.; Stich, D.; Ibañez, J.M.; Saccorotti, G. Multiplet Focal Mechanisms from Polarities and Relative Locations: The Iznajar Swarm in Southern Spain. *Bull. Seismol. Soc. Am.* **2009**, *99*, 3421–3429. [CrossRef]
109. Stich, D.; Ammon, C.J.; Morales, J. Moment Tensor Solutions for Small and Moderate Earthquakes in the Ibero-Maghreb Region. *J. Geophys. Res. Solid. Earth* **2003**, *108*, 2148. [CrossRef]
110. Pedrera, A.; Marín-Lechado, C.; Stich, D.; Ruiz-Constán, A.; Galindo-Zaldívar, J.; Rey-Moral, C.; de Lis Mancilla, F. Nucleation, Linkage and Active Propagation of a Segmented Quaternary Normal-Dextral Fault: The Loma Del Viento Fault (Campo de Dalías, Eastern Betic Cordillera, SE Spain). *Tectonophysics* **2012**, *522–523*, 208–217. [CrossRef]
111. Marín-Lechado, C.; Galindo-Zaldívar, J.; Gil, A.J.; Borque, M.J.; de Lacy, M.C.; Pedrera, A.; López-Garrido, A.C.; Alfaro, P.; García-Tortosa, F.; Ramos, M.I.; et al. Levelling Profiles and a GPS Network to Monitor the Active Folding and Faulting Deformation in the Campo de Dalias (Betic Cordillera, Southeastern Spain). *Sensors* **2010**, *10*, 3504–3518. [CrossRef]
112. Galindo-Zaldívar, J.; Borque, M.J.; Pedrera, A.; Marín-Lechado, C.; Gil, A.J.; López-Garrido, A.C. Deformation Behaviour of the Low-Rate Active Balanegra Fault Zone from High-Precision Levelling (Betic Cordillera, SE Spain). *J. Geodyn.* **2013**, *71*, 43–51. [CrossRef]
113. Martínez-Martínez, J.M.; Booth-Rea, G.; Azañón, J.M.; Torcal, F. Active Transfer Fault Zone Linking a Segmented Extensional System (Betics, Southern Spain): Insight into Heterogeneous Extension Driven by Edge Delamination. *Tectonophysics* **2006**, *422*, 159–173. [CrossRef]
114. Martín, R.; Stich, D.; Morales, J.; Mancilla, F. Moment Tensor Solutions for the Iberian-Maghreb Region during the IberArray Deployment (2009–2013). *Tectonophysics* **2015**, *663*, 261–274. [CrossRef]
115. Etchecopar, A.; Vasseur, G.; Daignieres, M. An Inverse Problem in Microtectonics for the Determination of Stress Tensors from Fault Striation Analysis. *J. Struct. Geol.* **1981**, *3*, 51–65. [CrossRef]
116. Galindo Zaldívar, J.; González Lodéiro, F. Determinaciones de Estados de Esfuerzo a Partir de Fallas: Aplicación al Sector Occidental de Sierra Nevada. In *II Congreso Geológico de España*; Instituto Geológico y Minero de España: Madrid, Spain, 1988; Volume 2, pp. 145–148.
117. Angelier, J.; Mechler, P. Sur Une Méthode Graphique de Recherche des Contraintes Principales Également Utilisable en Tectonique et en Seismologie: La Methode des Diedres Droits. *Bull. Soc. Géol. Fr.* **1977**, *7*, 1309–1318.
118. Gephart, J.W.; Forsyth, D.W. An Improved Method for Determining the Regional Stress Tensor Using Earthquake Focal Mechanism Data: Application to the San Fernando Earthquake Sequence. *J. Geophys. Res.* **1984**, *89*, 9305–9320. [CrossRef]
119. Madarieta-Txurruka, A.; González-Castillo, L.; Peláez, J.A.; Catalán, M.; Henares, J.; Gil, A.J.; Lamas-Fernández, F.; Galindo-Zaldívar, J. The Role of Faults as Barriers in Confined Seismic Sequences: 2021 Seismicity in the Granada Basin (Betic Cordillera). *Tectonics* **2022**, *41*, e2022TC007481. [CrossRef]
120. Delvaux, D.; Sperner, B. New Aspects of Tectonic Stress Inversion with Reference to the TENSOR Program. *Geol. Soc. Spec. Publ.* **2003**, *212*, 75–100. [CrossRef]
121. Delvaux, D.; Barth, A. African Stress Pattern from Formal Inversion of Focal Mechanism Data. *Tectonophysics* **2010**, *482*, 105–128. [CrossRef]
122. Burg, J.P.; Célérier, B.; Chaudhry, N.M.; Ghazanfar, M.; Gnehm, F.; Schnellmann, M. Fault Analysis and Paleostress Evolution in Large Strain Regions: Methodological and Geological Discussion of the Southeastern Himalayan Fold-and-Thrust Belt in Pakistan. *J. Asian Earth Sci.* **2005**, *24*, 445–467. [CrossRef]
123. Célérier, B. *FSA: Fault and Stress Analysis Software, Version 33.8*; Université de Montpellier: Montpellier, France, 2011; Volume 2.
124. Lozano, L.; Cantavella, J.V.; Gaite, B.; Ruiz-Barajas, S.; Antón, R.; Barco, J. Seismic Analysis of the 2020–2021 Santa Fe Seismic Sequence in the Granada Basin, Spain: Relocations and Focal Mechanisms. *Seismol. Res. Lett.* **2022**, *93*, 3246–3265. [CrossRef]
125. Stich, D.; Alguacil, G.; Morales, J. The Relative Locations of Multiplets in the Vicinity of the Western Almería (Southern Spain) Earthquake Series of 1993–1994. *Geophys. J. Int.* **2001**, *146*, 801–812. [CrossRef]
126. Stich, D.; Batlló, J.; Morales, J.; Macià, R.; Dineva, S. Source Parameters of the Mw = 6.1 1910 Adra Earthquake (Southern Spain). *Geophys. J. Int.* **2003**, *155*, 539–546. [CrossRef]
127. Morales, J.; Singh, S.K.; Ordaz, M. Analysis of the Granada (Spain) Earthquake of 24 June, 1984 (M = 5) with Emphasis on Seismic Hazard in the Granada Basin. *Tectonophysics* **1996**, *257*, 253–263. [CrossRef]
128. IGN Seismic Moment Tensor. Available online: https://www.ign.es/web/ign/portal/tensor-momento-sismico/ (accessed on 30 May 2023).
129. Montillet, J.-P.; Bos, M.S. *Geodetic Time Series Analysis in Earth Sciences*; Springer: Berlin/Heidelberg, Germany, 2020; ISBN 9783030217174.

130. Hreinsdóttir, S.; Freymueller, J.T.; Bürgmann, R.; Mitchell, J. Coseismic Deformation of the 2002 Denali Fault Earthquake: Insights from GPS Measurements. *J. Geophys. Res. Solid Earth* **2006**, *111*, B03308. [CrossRef]

131. Larson, K.M. GPS Seismology. *J. Geod.* **2009**, *83*, 227–233. [CrossRef]

132. Gil, A.J.; Galindo-Zaldívar, J.; Sanz de Galdeano, C.; Borque, M.J.; Sánchez-Alzola, A.; Martinez-Martos, M.; Alfaro, P. The Padul Normal Fault Activity Constrained by GPS Data: Brittle Extension Orthogonal to Folding in the Central Betic Cordillera. *Tectonophysics* **2017**, *712–713*, 64–71. [CrossRef]

133. Martin-Rojas, I.; Alfaro, P.; Galindo-Záldivar, J.; Borque, M.J.; García-Tortosa, F.J.; Sanz de Galdeano, C.; Avilés, M.; Sánchez-Alzola, A.; González-Castillo, L.; Ruano, P.; et al. Insights of Active Extension within a Collisional Orogen from GNSS (Central Betic Cordillera, S Spain). *Tectonics* **2023**, *42*, e2022TC007723.

134. Reicherter, K.R.; Jabaloy, A.; Galindo-Zaldívar, J.; Ruano, P.; Becker-Heidmann, P.; Morales, J.; Reiss, S.; González-Lodeiro, F. Repeated Palaeoseismic Activity of the Ventas de Zafarraya Fault (S Spain) and Its Relation with the 1884 Andalusian Earthquake. *Int. J. Earth Sci.* **2003**, *92*, 912–922. [CrossRef]

135. Sanz de Galdeano, C.; Peláez, J.A.; López Casado, C. Seismic Potential of the Main Active Faults in the Granada Basin (Southern Spain). *Pure Appl. Geophys.* **2003**, *160*, 1537–1556. [CrossRef]

136. Martínez-Martos, M.; Galindo-Zaldívar, J.; Sanz de Galdeano, C.; García-Tortosa, F.J.; Martínez-Moreno, F.J.; Ruano, P.; González-Castillo, L.; Azañón, J.M. Latest Extension of the Laujar Fault in a Convergence Setting (Sierra Nevada, Betic Cordillera). *J. Geodyn.* **2017**, *104*, 15–26. [CrossRef]

137. Hamdache, M.; Henares, J.; Peláez, J.A.; Damerdji, Y. Fractal Analysis of Earthquake Sequences in the Ibero-Maghrebian Region. *Pure Appl. Geophys.* **2019**, *176*, 1397–1416. [CrossRef]

138. Udías, A.; Muñoz, D. The Andalusian Earthquake of 25 December 1884. *Tectonophysics* **1979**, *53*, 291–299. [CrossRef]

139. Ocaña, E. Spatial Analysis of Recent Seismic Activity in Southern Spain. Ph.D. Thesis, University of Granada, Granada, Spain, 2009.

140. Gràcia, E.; Bartolome, R.; Lo Iacono, C.; Moreno, X.; Stich, D.; Martínez-Diaz, J.J.; Bozzano, G.; Martínez-Loriente, S.; Perea, H.; Diez, S.; et al. Acoustic and Seismic Imaging of the Adra Fault (NE Alboran Sea): In Search of the Source of the 1910 Adra Earthquake. *Nat. Hazards Earth Syst. Sci.* **2012**, *12*, 3255–3267. [CrossRef]

141. Morales, J.; Serrano, I.; Vidal, F.; Torcal, F. The Depth of the Earthquake Activity in the Central Betics (Southern Spain). *Geophys. Res. Lett.* **1997**, *24*, 3289–3292. [CrossRef]

142. Santos-Bueno, N.; Fernández-García, C.; Stich, D.; Mancilla, F.d.L.; Martín, R.; Molina-Aguilera, A.; Morales, J. Focal Mechanisms for Subcrustal Earthquakes Beneath the Gibraltar Arc. *Geophys. Res. Lett.* **2019**, *46*, 2534–2543. [CrossRef]

143. Buforn, E.; Pro, C.; Cesca, S.; Udías, A.; del Fresno, C. The 2010 Granada, Spain, Deep Earthquake. *Bull. Seismol. Soc. Am.* **2011**, *101*, 2418–2430. [CrossRef]

144. Vidal, F. Sismotectónica de La Región Béticas-Mar de Alborán. Ph.D. Thesis, University of Granada, Granada, Spain, 1986.

145. Balanyá, J.C.; Crespo-Blanc, A.; Díaz-Azpiroz, M.; Expósito, I.; Torcal, F.; Pérez-Peña, V.; Booth-Rea, G. Arc-Parallel vs Back-Arc Extension in the Western Gibraltar Arc: Is the Gibraltar Forearc Still Active? *Geol. Acta* **2012**, *10*, 249–263. [CrossRef]

146. Serrano, I. Distribución Espacial de La Sismicidad En Las Cordilleras Béticas-Mar de Alborán. Ph.D. Thesis, University of Granada, Granada, Spain, 1999.

147. Garate, J.; Martin-Davila, J.; Khazaradze, G.; Echeverria, A.; Asensio, E.; Gil, A.J.; de Lacy, M.C.; Armenteros, J.A.; Ruiz, A.M.; Gallastegui, J.; et al. Topo-Iberia Project: CGPS Crustal Velocity Field in the Iberian Peninsula and Morocco. *GPS Solut.* **2015**, *19*, 287–295. [CrossRef]

148. Alfaro, P.; Sánchez-Alzola, A.; Martin-Rojas, I.; García-Tortosa, F.J.; Galindo-Zaldívar, J.; Avilés, M.; Garrido, A.C.L.; Sanz de Galdeano, C.; Ruano, P.; Martínez-Moreno, F.J.; et al. Geodetic Fault Slip Rates on Active Faults in the Baza Sub-Basin (SE Spain): Insights for Seismic Hazard Assessment. *J. Geodyn.* **2021**, *144*, 101815. [CrossRef]

149. Ruano, P.; Galindo-Zaldívar, J. Striated and Pitted Pebbles as Paleostress Markers: An Example from the Central Transect of the Betic Cordillera (SE Spain). *Tectonophysics* **2004**, *379*, 183–198. [CrossRef]

150. Ruiz-constán, A.; Galindo-zaldívar, J.; Martínez, M.A.; Pedrera, A.; Martínez-Martos, M. Estructura de La Cuenca de Ugíjar a Partir de Datos Gravimétricos y Magnéticos (Zonas Internas, Cordillera Bética Centra) Structure of the Ugíjar Basin Using Gravity and Magnetic Data (Internal Zones, Central Betic Cordillera). *Geogaceta* **2013**, *54*, 95–98.

151. Galindo-Zaldívar, J. Etapas de Fallamiento Neógenas En La Mitad Occidental de La Depresión de Ugíjar (Cordillera Béticas). *Estud. Geol.* **1986**, *42*, 1–10. [CrossRef]

152. Jabaloy, A.; Galindo-Zaldívar, J.; González-Lodeiro, F. The Alpujárride-Nevado-Filábride Extensional Shear Zone, Betic Cordillera, SE Spain. *J. Struct. Geol.* **1993**, *15*, 555–569. [CrossRef]

153. Mancilla, F.D.L.; Stich, D.; Berrocoso, M.; Martín, R.; Morales, J.; Fernandez-Ros, A.; Páez, R.; Pérez-Peña, A. Delamination in the Betic Range: Deep Structure, Seismicity, and GPS Motion. *Geology* **2013**, *41*, 307–310. [CrossRef]

154. Pérez-Peña, J.V.; Azañón, J.M.; Azor, A.; Booth-Rea, G.; Galve, J.P.; Roldán, F.J.; Mancilla, F.; Giaconia, F.; Morales, J.; Al-Awabdeh, M. Quaternary Landscape Evolution Driven by Slab-Pull Mechanisms in the Granada Basin (Central Betics). *Tectonophysics* **2015**, *663*, 5–18. [CrossRef]

155. Azañón, J.M.; Galve, J.P.; Pérez-Peña, J.V.; Giaconia, F.; Carvajal, R.; Booth-Rea, G.; Jabaloy, A.; Vázquez, M.; Azor, A.; Roldán, F.J. Relief and Drainage Evolution during the Exhumation of the Sierra Nevada (SE Spain): Is Denudation Keeping Pace with Uplift? *Tectonophysics* **2015**, *663*, 19–32. [CrossRef]

156. Galindo-Zaldívar, J.; Jabaloy, A.; González-Lodeiro, F.; Aldaya, F. Crustal Structure of the Central Sector of the Betic Cordillera (SE Spain). *Tectonics* **1997**, *16*, 18–37. [CrossRef]

157. Pérez-Peña, J.V.; Azor, A.; Azañón, J.M.; Keller, E.A. Active Tectonics in the Sierra Nevada (Betic Cordillera, SE Spain): Insights from Geomorphic Indexes and Drainage Pattern Analysis. *Geomorphology* **2010**, *119*, 74–87. [CrossRef]

158. Torne, M.; Fernàndez, M.; Comas, M.C.; Soto, J.I. Lithospheric Structure beneath the Alboran Basin: Results from 3D Gravity Modeling and Tectonic Relevance. *J. Geophys. Res. Solid. Earth* **2000**, *105*, 3209–3228. [CrossRef]

159. Guerra-Merchán, A.; Serrano, F.; Hlila, R.; El Kadiri, K.; Sanz de Galdeano, C.; Garcés, M. Tectono-Sedimentary Evolution of the Peripheral Basins of the Alboran Sea in the Arc of Gibraltar during the Latest Messinian-Pliocene. *J. Geodyn.* **2014**, *77*, 158–170. [CrossRef]

160. Martínez-Martínez, J.M. Lateral Interaction between Metamorphic Core Complexes and Less-Extended, Tilt-Block Domains: The Alpujarras Strike-Slip Transfer Fault Zone (Betics, SE Spain). *J. Struct. Geol.* **2006**, *28*, 602–620. [CrossRef]

161. Mancilla, F.d.L.; Heit, B.; Morales, J.; Yuan, X.; Stich, D.; Molina-Aguilera, A.; Azañón, J.M.; Martín, R. A STEP Fault in Central Betics, Associated with Lateral Lithospheric Tearing at the Northern Edge of the Gibraltar Arc Subduction System. *Earth Planet. Sci. Lett.* **2018**, *486*, 32–40. [CrossRef]

162. Bessiere, E.; Jolivet, L.; Augier, R.; Scaillet, S.; Precigout, J.; Azanon, J.M.; Crespo-Blanc, A.; Masini, E.; Do Couto, D. Lateral Variations of Pressure-Temperature Evolution in Non-Cylindrical Orogens and 3-D Subduction Dynamics: The Betic-Rif Cordillera Example. *BSGF Earth Sci. Bull.* **2021**, *192*, 8. [CrossRef]

163. Barranco, L.M.; Ansorge, J.; Banda, E. Seismic Refraction Constraints on the Geometry of the Ronda Peridotitic Massif (Betic Cordillera, Spain). *Tectonophysics* **1990**, *184*, 379–392. [CrossRef]

164. Banda, E.; Gallart, J.; García-Dueñas, V.; Dañobeitia, J.J.; Makris, J. Lateral Variation of the Crust in the Iberian Peninsula: New Evidence from the Betic Cordillera. *Tectonophysics* **1993**, *221*, 53–66. [CrossRef]

165. Torné, M.; Banda, E.; García-Dueñas, V.; Balanyá, J.C. Mantle-Lithosphere Bodies in the Alboran Crustal Domain (Ronda Peridotites, Betic-Rif Orogenic Belt). *Earth Planet. Sci. Lett.* **1992**, *110*, 163–171. [CrossRef]

166. Tendero-Salmerón, V.; Lafosse, M.; d'Acremont, E.; Rabaute, A.; Azzouz, O.; Ercilla, G.; Makkaoui, M.; Galindo-Zaldivar, J. Application of Automated Throw Backstripping Method to Characterize Recent Faulting Activity Migration in the Al Hoceima Bay (Northeast Morocco): Geodynamic Implications. *Front. Earth Sci.* **2021**, *9*, 645942. [CrossRef]

167. Tendero-Salmerón, V.; Galindo-Zaldívar, J.; d'Acremont, E.; Catalán, M.; Martos, Y.M.; Ammar, A.; Ercilla, G. New Insights on the Alboran Sea Basin Extension and Continental Collision from Magnetic Anomalies Related to Magmatism (Western Mediterranean). *Mar. Geol.* **2022**, *443*, 106696. [CrossRef]

168. Azañón, J.M.; Pérez-Peña, J.V.; Giaconia, F.; Booth-Rea, G.; Martínez-Martínez, J.M. Tectónica Activa En La Cordillera Bética Oriental y Central Mediante Análisis Morfotectónico: El Caso de Sierra Nevada y Sierra Alhamilla. *J. Iber. Geol.* **2012**, *38*, 239–253. [CrossRef]

169. Pedrera, A.; Ruiz-Constán, A.; Marín-Lechado, C.; Galindo-Zaldívar, J.; González, A.; Peláez, J.A. Seismic Transpressive Basement Faults and Monocline Development in a Foreland Basin (Eastern Guadalquivir, SE Spain). *Tectonics* **2013**, *32*, 1571–1586. [CrossRef]

170. Morales, J.; Azañón, J.M.; Stich, D.; Roldán, F.J.; Pérez-Peña, J.V.; Martín, R.; Cantavella, J.V.; Martín, J.B.; Mancilla, F.; González-Ramón, A. The 2012-2013 Earthquake Swarm in the Eastern Guadalquivir Basin (South Spain): A Case of Heterogeneous Faulting Due to Oroclinal Bending. *Gondwana Res.* **2015**, *28*, 1566–1578. [CrossRef]

171. Gómez de la Peña, L.; Ranero, C.R.; Gràcia, E.; Booth-Rea, G.; Azañón, J.M.; Tinivella, U.; Yelles-Chaouche, A. Evidence for a Developing Plate Boundary in the Western Mediterranean. *Nat. Commun.* **2022**, *13*, 4786. [CrossRef] [PubMed]

172. Ma, C.; Foster, D.A.; Hames, W.E.; Mueller, P.A.; Steltenpohl, M.G. From the Alleghanian to the Atlantic: Extensional Collapse of the Southernmost Appalachian Orogen. *Geology* **2019**, *47*, 367–370. [CrossRef]

173. Andersen, T.B.; Bj0m, J. Uplift of Deep Crust during Orogenic Extensional Collapse: Amodel Based on Field Studies in the Song-Sunnfjord Region of Western Normay. *Tectonics* **1990**, *9*, 1097–1111.

174. Menant, A.; Sternai, P.; Jolivet, L.; Guillou-Frottier, L.; Gerya, T. 3D Numerical Modeling of Mantle Flow, Crustal Dynamics and Magma Genesis Associated with Slab Roll-Back and Tearing: The Eastern Mediterranean Case. *Earth Planet. Sci. Lett.* **2016**, *442*, 93–107. [CrossRef]

175. Fadil, A.; Vernant, P.; McClusky, S.; Reilinger, R.; Gomez, F.; Ben Sari, D.; Mourabit, T.; Feigl, K.; Barazangi, M. Active Tectonics of the Western Mediterranean: Geodetic Evidence for Rollback of a Delaminated Subcontinental Lithospheric Slab beneath the Rif Mountains, Morocco. *Geology* **2006**, *34*, 529–532. [CrossRef]

176. D'Agostino, N.; D'Anastasio, E.; Gervasi, A.; Guerra, I.; Nedimović, M.R.; Seeber, L.; Steckler, M. Forearc Extension and Slow Rollback of the Calabrian Arc from GPS Measurements. *Geophys. Res. Lett.* **2011**, *38*, L17304. [CrossRef]

177. Brun, J.P.; Faccenna, C.; Gueydan, F.; Sokoutis, D.; Philippon, M.; Kydonakis, K.; Gorini, C. The Two-Stage Aegean Extension, from Localized to Distributed, a Result of Slab Rollback Acceleration. *Can. J. Earth Sci.* **2016**, *53*, 1142–1157. [CrossRef]

178. Shaw, B.; Jackson, J. Earthquake Mechanisms and Active Tectonics of the Hellenic Subduction Zone. *Geophys. J. Int.* **2010**, *181*, 966–984. [CrossRef]

179. Polonia, A.; Torelli, L.; Mussoni, P.; Gasperini, L.; Artoni, A.; Klaeschen, D. The Calabrian Arc Subduction Complex in the Ionian Sea: Regional Architecture, Active Deformation, and Seismic Hazard. *Tectonics* **2011**, *30*, TC5018. [CrossRef]
180. Spakman, W.; Hall, R. Surface Deformation and Slab-Mantle Interaction during Banda Arc Subduction Rollback. *Nat. Geosci.* **2010**, *3*, 562–566. [CrossRef]